EXPERIMENTAL INVESTIGATION OF LASER SCAN STRATEGY ON THE MICROSTRUCTURE, MECHANICAL PROPERTIES AND RESIDUAL STRESS OF INCONEL 718 PARTS FABRICATED BY SELECTIVE LASER MELTING

by

KIRITI MAMIDI

Presented to the Faculty of the Graduate School of

The University of Texas at Arlington

in partial fulfillment of the requirements

for the degree of

MASTER OF SCIENCE IN MECHANICAL ENGINEERING

THE UNIVERSITY OF TEXAS AT ARLINGTON

August 2020

Acknowledgment

Firstly, I am truly grateful to Dr. Narges Shayesteh for being patient and trusting me with the equipment of the Innovative Additive Manufacturing lab. Being able to work under her was a fantastic learning experience as she has immense knowledge and an undying motivation for research during tough times, which in turn kept me motivated. This research endeavor would not have been possible without the generous support and invaluable guidance of Dr. Amirhesam Amerinatanzi throughout the project.

I sincerely thank my colleagues Mr. Bharath Bhushan Ravichander, along with Mr. Behzad Farhang, who helped me fabricate parts for this project despite their busy schedule and assisting me in every step during the research. An exceptional thanks to Mr. Vignesh Ram Kumar Rajendran for associating in research and providing valuable results, inputs, and constructive ideas for the project. I glad to have worked with Mr. Himanth Kumar Talla, Mr. Srihari Srivathsan, and Mr. Sourabh Thakare, who provided their honest and genuine comments on my work when asked for. On the same note, I would like to thank Mr. Vijay Gopal and Dr. Umang Dighe for their support and inspiring and motivating me to undertake research.

Furthermore, I would also like to thank the members of my committee: Dr. Amir Ameri and Dr. Chen Kan for their time, inputs and for providing me with their valuable feedback and Mr. Rex Winfrey, Mr. Vedant Chahal and Mr. Kermit Beird for allowing me to use their lab equipment as and when necessary.

Finally, I heartfully thank all my friends for their camaraderie and memories forged over the past couple of years. I am always indebted to my family and my uncle for their belief in my caliber and their encouragement to further pursue my academic interests by supporting me financially and otherwise.

On the shoulders of giants

Abstract

EXPERIMENTAL INVESTIGATION OF LASER SCAN STRATEGY ON THE MICROSTRUCTURE, MECHANICAL PROPERTIES AND RESIDUAL STRESS OF INCONEL 718 PARTS FABRICATED BY SELECTIVE LASER MELTING

Kiriti Mamidi, M.S

The University of Texas at Arlington, 2020

Supervising Professor: Dr. Narges Shayesteh

Inconel 718 (IN718) is a nickel-based superalloy which exhibits excellent tensile and impact resistant properties along with good corrosion resistance at high temperatures. However, due to the high toughness and work hardening, the machinability of this superalloy is low. Therefore, the selective laser melting (SLM) process has been adopted as an efficient technique to fabricate IN718 parts as it overcomes the problems associated with conventional manufacturing of superalloys. SLM is a widely used additive manufacturing technique which offers the possibility to induce multi-functionality into a single component, and thus reduce the number of components that are needed.

In the SLM process, various process parameters like scan strategy, laser power, scan speed, and energy density are defined for the fabrication to regulate the microstructure and thus control the mechanical properties like tensile strength, yield strength, impact strength, and hardness. Owing to the nature of the SLM process, there are consistent repetitions of thermal cycles, which in turn induce residual stress into the part. These residual stresses can be detrimental to the microstructure and hence mechanical properties of the part. Residual stresses lead to warping of the part during the fabrication process, thereby leading to failure of the component. Although each process parameter has an independent and definitive effect on the overall mechanical and metallurgical properties, scan strategy is an independent process parameter which directly affects the level of residual stresses, microstructure, and mechanical properties of the SLM part, as the heat zones in part can be shifted from location to another by varying the scan strategy. This variation of the area of the heat zone changes the temperature gradient, which thereby determines the grain size ranging

from equiaxed to elongated. Hence, the scan strategy is the only parameter that is varied for this study. The various scan strategies adopted here are checkered, stripes, FO1, and customized scan strategy, where the angle between the consecutive layers has been changed consistently at an angle of 90^{o}.

In this study, the residual stress was deduced using methods like hardness, X-ray powder diffraction (XRD), and direct method (CMM) followed by microstructural and compositional analysis on the parts. Mechanical testing like compression tests, hardness test, and roughness test was performed on the SLM fabricated parts. This effort was undertaken to identify the effect of scan strategy on residual stress and to discuss the metallurgical interactions between the mechanical and microstructural properties within the IN718 superalloy.

Table of Contents

List of Tables

List of Figures

Chapter 1. Introduction

1.1. Motivation

Residual stresses in additively manufactured parts affect the component adversely. The probability of delamination between layers of the part is high when the residual stresses are high. Although additive manufacturing offers great flexibility in design, the computer-aided-design (CAD) conformation may get affected due to the defects induced because of residual stress. Therefore, the study of the influence of fabrication parameters like scan strategy on microstructural and mechanical properties aids in understanding the structure of residual stress generation. In addition to finding the residual stresses, the relation between microstructure and mechanical properties, and their effect on residual stresses can be quantified. This comprehension of the residual stress generation and its correlation with the scan strategy provides feasibility to control the build process dynamically, thereby reducing the post-processing operations for stress relief.

1.2. Objectives

This work primarily focusses on the effect of various scan strategies on the generation of residual stresses and their effect on microstructure and mechanical properties of parts fabricated on an EOS M290 machine. In addition to the above-discussed motivation, it is also rational to discern the underlying process-structure-property relationships, potentially enabling the use of additive manufacturing (AM) for parts with novel functional properties. As the microstructural properties like grain size affect the mechanical properties, their impact on the residual stresses is also pronounced. This comprehension of the interrelation between the earlier discussed properties may provide a larger number of control variables while designing the process, thereby making the fabrication process more efficient. Therefore, the co-relations between the metallurgical, mechanical properties, and the residual stresses have also been studied.

1.3. Approach

Initially, a comprehensive literature review has been done to understand: (i) the basic properties of IN718 samples fabricated using selective laser melting (SLM) processes; (ii) the microstructural,

mechanical properties, and residual stresses of SLM IN718 alloys; (iii) the available techniques for measurement of residual stress in IN718 alloys; (iv) the effect of various process parameters variation on the properties of the alloy; and (v) the effect of varying the scan strategy exclusively on the microstructural and mechanical properties in connection with their impact on residual stress. An initial effort was conducted to arrive at the optimum process parameters (e.g., laser powder *P*, hatch spacing *h*, scanning speed *v*) for fabrication in such a way to introduce stable microstructure and texture within the SLM IN718 specimens. Following the fabrication of the IN718 samples, coordinate-measuring machine (CMM) was used to obtain the deflection and hence residual stress values. Residual stress values were also calculated through XRD and hardness analysis. Next, a series of scanning electron microscopy (SEM) observations were performed to obtain the microstructure of the parts fabricated with different scan strategies. Mechanical testing was subsequently performed to understand the behavior of the SLM fabricated part under various physical strains. Finally, the results were interpreted to understand the influence of the scanning strategy on the residual stress formation and hence microstructure and mechanical properties of the SLM IN718 specimens.

1.4. Outline

Chapter 1 presents the rationale of the research building upon the literature review conducted in further chapters. A synopsis of the project can be obtained from the first chapter.

Chapter 2 provides a detailed review of literature that covers the work done previously and describes any possible avenues for furthering research as an overview. Section 2.1 discusses the history of the IN718 material and its applications in SLM. Section 2.2 provides an overview of SLM in general and the usability of IN718. General discussions on the microstructural and mechanical properties of SLM IN718 are also discussed in sections 2.3 and 2.4, respectively. Proceeding further, in section 2.5, the trends of residual stress generation and the causes of the residual stress are discussed. The process optimization methods to minimize the generation of residual stresses in SLM parts are finally discussed in section 2.6.

Chapter 3 discusses the process by which the parts are developed for fabrication, wherein the design is initially conceived considering the end application from a research perspective (section 3.1). Section 3.2

discusses powder preparation and fabrication. Section 3 discusses the experimental procedures adopted for the microstructure, metallurgical, and mechanical characterization, namely SEM, hardness, roughness, XRD, and CMM.

Chapter 4 discusses the results of the proposed work. Sections 4.1-3 discusses the results and discussions on microstructure, hardness, and XRD analyses. The results from the residual stress evaluation are also discussed in section 4.4.

Chapter 5 covers the conclusions and the avenues for further progressing the research.

1.5. Contribution

Following the completion, this work contributes towards:

1. An understanding of the effect of scanning strategy on the residual stress, microstructure, composition, and mechanical properties of SLM IN718.
2. Identifying the possible dependence of the residual stress on the mechanical and microstructural properties of IN718 material.

1.6. Publications

1. Rajendran VR, Mamidi K, Ravichander B, Farhang B, Amerinatanzi A, Moghaddam NS. Determination of residual stress for Inconel 718 samples fabricated through different scanning strategies in selective laser melting. InBehavior and Mechanics of Multifunctional Materials IX 2020 May 21 (Vol. 11377, p. 1137719). International Society for Optics and Photonics.
2. Mamidi K, Talla HK, Ravichander BB, Farhang B, Moghaddam NS, Amerinatanzi A. Study on the influence of post-processing parameters over microstructure and metallurgical properties of NiTi alloy. InBehavior and Mechanics of Multifunctional Materials IX 2020 May 18 (Vol. 11377, p. 113770V). International Society for Optics and Photonics.

Chapter 2. Background and Literature Review

2.1. IN718 Superalloys

2.1.1. History of IN718 Superalloys

IN718 is a nickel-base superalloy that was developed by the International Nickel Company in 1959. The high-temperature applications of gas turbine technology necessitated a material to withstand high temperatures and retain the stipulated mechanical and metallurgical properties [1-3]. The IN718 alloy was initially introduced into mainstream high-temperature technology by P&W in the early 1960s. The further development of the alloy has enabled the manufacturing of lightweight and economical engines. Owing to its resistance to variation in mechanical and chemical, IN718 was used in the diffuser case of SR-71 Blackbird. As IN718 exhibits these above-stated high-temperature performance characteristics, it is classified as a superalloy [4]. The resistance to degradation of mechanical properties of IN718 at high temperatures has found in a wide range of applications [5]. The necessity to replace the extensive usage of iron and aluminum alloys in aerospace as they pose a compromise in lightweight and integral strength saw an increase in demand for furthering the research for IN718 [6].

2.1.2. Chemistry and Phase Formation of IN718

IN718 constitutes Nickel as the primary constituent element. To augment the characteristics, elements like Fe, Cr, Nb, Mo, and Ti were used. Table 1 reports the common phases observed in IN718 superalloys. The three primary constituent phases of the alloy are γ, γ', γ", and δ [7]. The alloying phases are comprised of precipitates created by the fusion of alloying matrix with the constituent elements. The phases can be differentiated by a disparity in the atomic size. γ phase primarily comprises the Nickel. γ' phase consists of precipitates of Nickel with elements like Al, Ti, Nb, which differ in size by 6-18% when compared to the primary alloying matrix. The occurrence of definitive grain boundaries can be attributed to the presence of Carbon as its atomic diameter differs by more than 20% [7-9].

The γ phase of IN718 is an austenitic, face-centered crystal lattice [10, 11]. Most of the Nickel-based superalloys are constituted of the above-stated γ phase. The γ' is termed as the primary strengthening

phase [12, 13]. The γ' is the strengthening phase made of precipitates formed by Titanium and Niobium. As the lattice and chemical compatibility of γ and γ' is high, the precipitate is distributed throughout the matrix uniformly, thereby imparting stability against dispersion [7]. The γ" phase is another phase of IN718. Comprising of a BCT crystal structure, Niobium in IN718 is responsible for enhanced strength in the superalloy [13]. The fineness of the precipitate particles is of primordial importance as the ductility decreases when the precipitation hardening is increased. The δ phase of IN718 is the transformed phase of γ". Both δ and γ" share a typical composition, but a difference in the crystal structure is observed [14]. Due to the difference in the crystal structure, the yield properties of the part are reduced [15, 16]. Extreme high temperature shall influence the microstructure by converting the γ" to the δ phase, which reduces the strength of the alloy specimen [17-20].

Table 1. The primary constituent phases of IN718 alloy [17-20].

Phase	Crystal structure	Chemical formula
γ	Face Centered Cube	Ni
γ′	Face Centered Cube	Ni_3(Al, Ti)
γ″	Body-Centered Tetragonal	Ni_3Nb
δ	Orthorhombic	Ni_3Nb
MC	Cubic	(Nb,Ti)C
Laves	Hexagonal	$(Ni,Fe,Cr)_2(Nb,Mo,Ti)$

2.1.3. Traditional Manufacturing of IN718

IN718 can be manufactured using various fabrication techniques. As the compositional and the grain structure can significantly influence the applicability of the alloy specimen, it is necessary to choose an appropriate manufacturing process.

Casting is a commonly used fabrication procedure for Nickel alloys as the parts manufactured by casting have better grain flow and less-fine grain structure [21]. Although porosity is induced into the cast part, it can be reduced by post-process treatments like Hot Isostatic Pressing. However, the formation of

Laves and other precipitate phases which consume the other alloying elements, cannot be directly countered by casting [10]. The cast alloy specimen metallurgical properties can be changed by wrought treatment techniques. Wrought IN718 is manufactured either by cold or heat treatment of the cast or raw billet of IN718, where mechanical forces are applied on the alloy ingot to refine the grain structure [22].

Powder metallurgy is another potential fabrication technique of IN718 [23]. This fabrication technique is used to produce a high specimen with high dimensional accuracy with near-net shapes. The grain structure in powder metallurgy is more refined and uniform when compared to wrought or cast processes [23]. Although the desired mechanical and metallurgical properties can be obtained using casting and powder metallurgy techniques, the post-processing heat treatment operations create oxides like Al_2O_3 and TiO_2, which enhance the brittleness of the part [24, 25]. This reduces the ductility of the part at elevated temperatures.

Therefore, additive manufacturing (AM) technologies like selective laser melting (SLM) and direct energy deposition (DED) are proven to be better fabrication procedures [26, 27]. The flexibility of the process, i.e., the ability to regulate various process parameters to tailor the application-specific grain structure dramatically enhances the potential for AM to be adopted as the standardized fabrication technique [24].

2.2.Metal Additive Manufacturing

2.2.1. Introduction and History

The AM technique is an emerging technology where the initial primary aim was to fabricate working prototypes for the actual end application parts [28-32]. As the name suggests, the process approach is to build the specimen dynamically using multiple layers of the target material by stacking them one over the other [33]. Charles W. Hull of 3D systems corporation developed the first working 3d printer in 1984 [34]. Polymer materials were used at the outset of additive manufacturing as they were less tedious to fabricate and more readily available [28, 35, 36]. This process came to be known as Stereolithography. The

AM processes have significantly evolved with time, finding applications in aerospace and biomedical engineering. This was possible as the number of feasible material options exploded with the development of novel processes like selective laser sintering (SLS), stereolithography (SLA). Research to use powder materials drove the emergence of SLS [37, 38] at the University of Texas, which was later termed as Powder bed manufacturing [39]. In the 1990s, Dr. Hans J. Langer founded EOS where a direct metal laser sintering (DMLS) machine known as the EOS M250 was developed [40]. This process was later translated to fabricate complex metal specimen efficiently. The variation of heat source was necessary to control the material interactions [37, 38]. On the same lines, Anderson and Larson developed a new AM technique called electron beam melting (EBM) [41]. The onset of the AM revolution began when the open-source fused deposition modeling (FDM) printer was commercialized.

2.2.2. Benefits and Challenges

AM techniques evolved with time and were inducted into mainstream fabrication. Although initially AM was intended to be limited to rapid prototyping, over time, research aided to realize the potential of the fabrication technique. The majority of the AM process currently being used have minimized the human-machine interaction, which thereby significantly reduced the idle times during fabrication. This reduction in redundancy has proven the process to be more economical [37, 38]. Extremely complex parts like rocket nozzles demand high precision fabrication procedures as the failure of such components can be catastrophic. The number of required machining operations is significantly higher as the part geometric becomes more complex [42]. This complexity can be addressed using AM [33]. As AM is a layer-based process, the intricacies of the designed part can be withheld without the loss of the design intent of the part. Conventionally fabricated parts using manufacturing techniques like turning and milling need further excellent finishing operations like honing and lapping, thereby increasing the operation costs. AM processes also help eliminate the necessity of assemblies as compliant mechanisms can be fabricated using AM processes [42]. Considering the advantages of AM processes, it is also worthwhile to study the downsides of the process as well, as it provides us with a more comprehensive understanding of the process. The

customized process settings in AM make the process take a longer time for fabrication [40]. However, this must not be mistaken for the idle times in conventional fabrication processes. The initial installation costs are also high for some AM techniques. Skilled machine engineers are still needed to oversee the fabrication procedure to troubleshoot in case of fabrication failures. Like any other fabrication process, the number of parts that can be fabricated is resource-limited [33].

2.2.3. Classification of Additive Manufacturing Technology

As the study is related to metal printing, the most prominent respective metal AM techniques are discussed. Various heating sources like laser, electron beam, and ultrasonic vibrations can be used to fabricate the part using AM principles [43]. There are numerous AM techniques available for manufacturing based on the type of feed material structure. They can be classified into powder-based and flow-based (direct energy deposition) methods, as seen in Figure 1 [44]. The powder bed-based method uses fine powder particles as feed material. Flow-based techniques can utilize both wire and powder feed systems. Powder bed-based techniques are considered more accurate systems as the powder particles are small, thereby reducing the geometrical deviation and provide better surface finish [44, 45]. However, on the other hand, flow-based techniques are faster and are economical as the material wastage is virtually minimum [46]. Figure 2 shows the classification of additive manufacturing techniques.

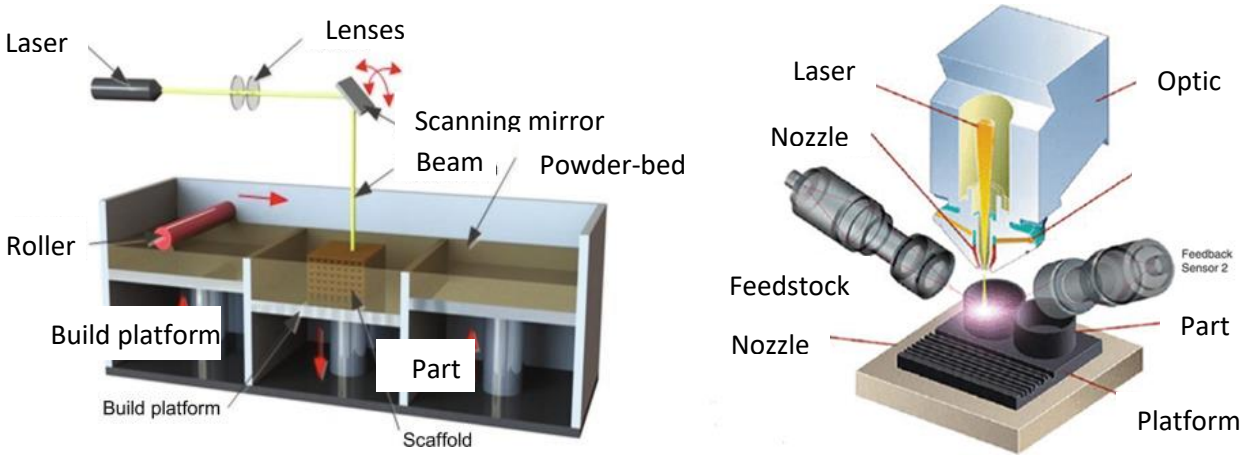

Figure 1: The schematic of powder-bed based and flow-based techniques [47, 48].

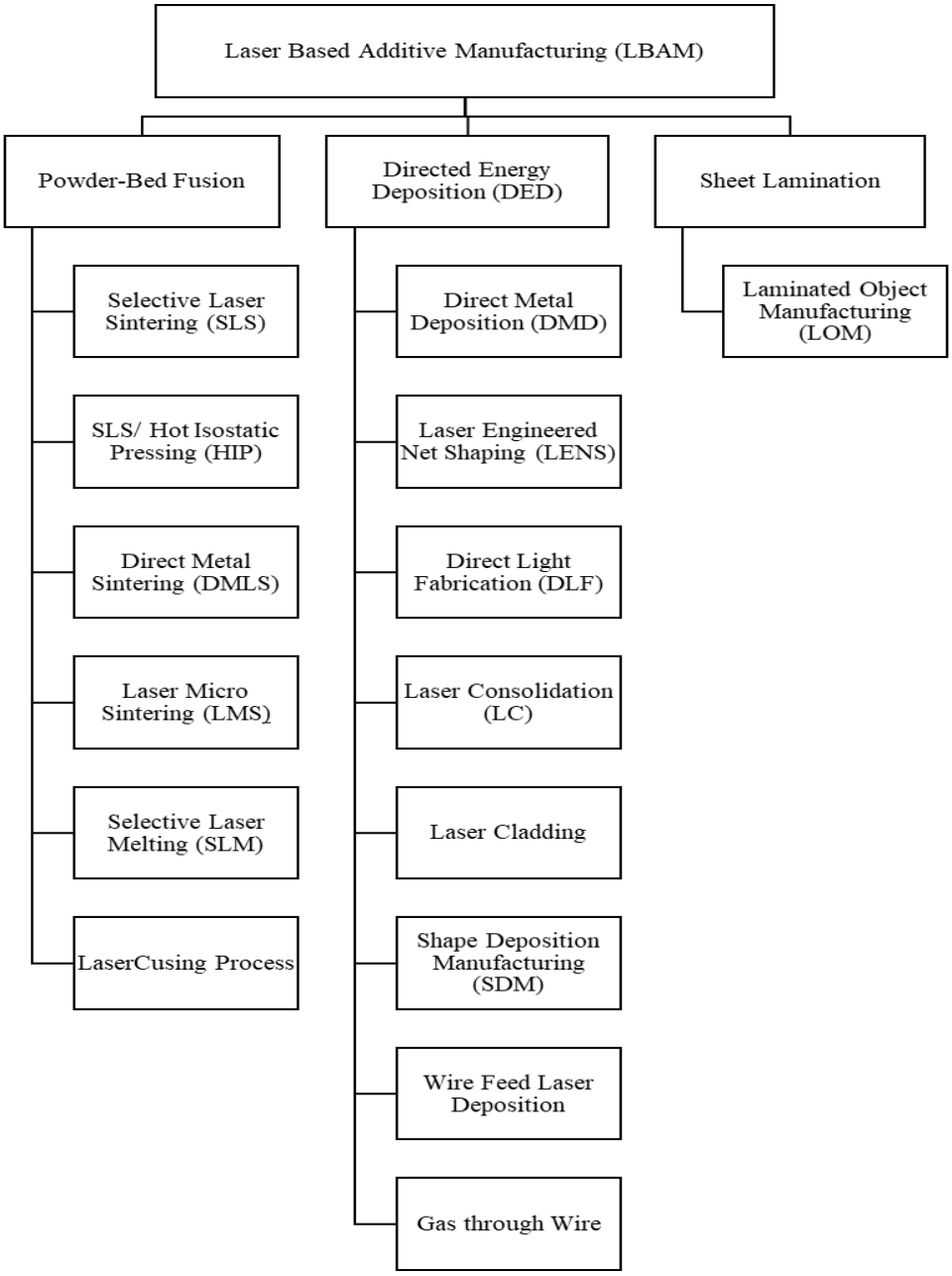

Figure 2: Classification of Laser-Based Additive Manufacturing (LBAM) techniques [47].

2.2.3.1. Flow-based methods

The flow-based techniques employ a pressure regulated converging nozzle to deliver the raw feed material at the point of laser impact [49-52]. The flow of feed powder is regulated using pressurized gas delivery system. The laser is placed at the center of the nozzle system. The offset of the laser can directly impact the heat zones created in the part. A servo controller is used to move the nozzle in the three-

dimensional axes [53]. The build plate is usually restricted to motion in horizontal axes. The various Flow-based techniques are:

- Direct metal deposition (DED)
- Laser engineered net shaping (LENS)
- Direct laser fabrication (DLF)
- Laser consolidation (LC)
- Laser cladding

2.2.3.2. Powder bed-based methods

The powder bed-based techniques use a build plate to fabricate the parts. The powder is spread evenly across the substrate or the build plate. The amount of powder layer spread depends on the layer thickness of the fabrication procedure. The target specimen along with the designed support structure are printed on the substrate. To accommodate the new layer, the substrate is moved down by one-layer thickness height. The similar process is continued till the whole part is fabricated successfully [34].

(i) Selective laser sintering (SLS)

Dr. Joe Beaman at the university of Texas at Austin developed the Selective laser Sintering technique in the 1980s [54]. Selective laser sintering can be done by partial melting or complete liquid sintering. Chemical sintering is a method of SLS where a chemical binder is used to bind and sinter the powder particles together (See Figure 3). The powder particles are melted using a laser [55]. The binder adheres to the powder particles together and begin to solidify after the laser pass is completed [56]. In this process, the laser energy is used to melt binder but not to melt the powder particles. The parts which are fabricated by this process are 505 porous and are termed as green parts. The parts are made fully dense only after treating heat treatment procedures are complete [57-59].

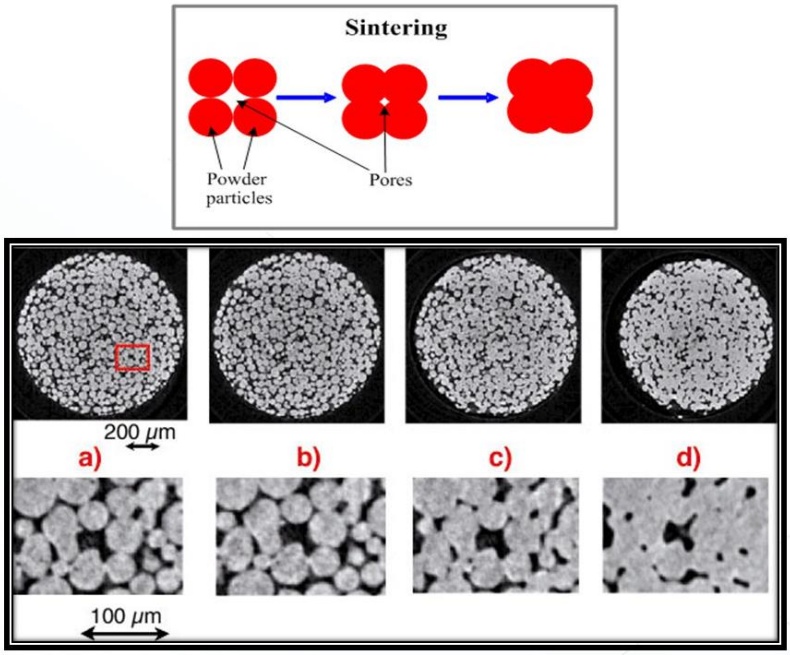

Figure 3: Selective Laser Sintering (SLS) Process method [60].

(ii) Direct metal laser sintering (DMLS)

The Direct metal laser sintering (DMLS) process was developed by Rapid Product Innovations (RPI) and EOS GmbH [61]. The feed form of the powder can be of varying grain morphology as it can still be used to fabricate alloy samples. This procedure provides flexibility to use powders which differ greatly in their chemical variation [59]. This is a high energy process, there by producing parts with high densities [62]. The high-density parts indicate the absence of internal defects in the part, thereby reducing both porosity and balling effect.

(iii) Selective laser melting

The SLM technique is an evolved AM process by which parts with high geometrical complexities can be fabricated which are approximately 100% dense [28, 63-80]. As the parts produced are highly dense, the necessity for heat treatment is eliminated [63]. The SLM process is like the SLS process in principle [81-91]. However, in SLM a laser of higher energy is employed, there by completely melting the powder particles [81, 92]. Although the SLM process produces highly dense parts, the parts manufactured by this fabrication mechanism have high amount of internal stresses (residual stresses) leading to effects like

warping and delamination of layers within the part [93]. Build plate reheating and temperature regulation in the chamber are a few methods to control the generation of residual stress.

(iv) Hot isostatic pressing

Hot isostatic pressing (HIP) is fundamentally a post processing operation, usually used to reduce porosity in the parts at high temperatures. Research at University of Texas developed and modified the process into a hybrid fabrication process which combines HIP and SLS techniques. This increases the rate of part production with holding the high-density feature of the part.

(v) Laser micro sintering

The laser micro sintering techniques was first proposed and developed by Laser Institute. Parts which are fabricated using this process have high resolution and significantly low surface roughness [94]. This fabrication technique is a modified version of Selective laser sintering technique. In LMS technique, the parts have significantly low surface roughness when compared to actual SLS process. However, it takes longer to fabricate the specimen using LMS [95, 96].

2.3.Selective Laser Melting of IN718

2.3.1. Microstructure in Selective Laser Melted IN718

The analysis of the microstructural properties of SLM fabricated IN718 is necessary to understand the melting and solidification processes [97]. The variation in the process parameters shall also induce many defects into the parts like porosities [98]. The microstructure of the part can be controlled as per the requirement if microstructure analysis is conducted. Scanning electron microscope (SEM), Transmission electron microscope (TEM), and optical microscopes can all be employed to obtain the microstructure of the specimen [97, 99]. The SLM process deals with continuous heating cooling cycles. This has a very distinctive effect on the grain structure [100]. Prolonged thermal exposure either due to high laser power or low scan speeds, shall produce elongated columnar grains. On the other hand, rapid heat loss can form equiaxed grains [18, 20, 100, 101]. Long columnar grains are usually found along the build direction of the

part. However, some studies [102] have reported the occurrence of non-columnar grains, which was later attributed to a variation in process parameters. The melt pool morphologies near substrate and top surface vary considerably. This is due to the higher rate of heat transfer at the top surface and lesser thermal interactions at the bottom surface [98]. The cooling rate at substrate is higher owing to the temperature gradient developed during the printing operation. The part thickness shall also affect the heat transfer rate in the sample as the rate of heat conduction varies throughout the part thickness [20, 101, 103].

2.3.2. Mechanical Properties in Selective Laser Melted IN718

The mechanical properties of IN718 are primarily necessary as the application of the fabricated part is often dependent on end use of the part [104-114]. Therefore, the use of SLM facilitates us to define and control the mechanical and metallurgical properties of the part [115]. A degradation in the properties like tensile and yield strength were observed [22, 100]. The difference in the characteristics is attributed to the variation in the governing process parameters [116]. The mechanical properties of the cast parts were observed to be inferior to that of wrought part [117, 118]. Homogenization of microstructure is observed in heat treated samples which are SLM fabricated [101]. The grain orientations can affect the nature of the parts in terms of ductility. Small and equiaxed grains augment the ductility of the part, whereas the columnar grains shall aid in enhancing the hardness of the alloy specimen [98]. However, in conjunction with the compositional study of the alloy, hardness and tensile mechanical tests give out a valid interpretation to the idea of choosing SLM for fabrication of IN718 alloy specimen [101]. The tensile properties of IN718 fabricated using SLM techniques were like that of the wrought specimen [119]. This is due the energy imparted to the metal powder shall mimic the effects of heat treatment if prolonged exposure or low scan speeds are used.

The process parameters of the SLM technique play a big role in determining the hardness of fabricated IN718 parts [100]. Studies have previously stated that the hardness of the SLM built part depend on the energy density of the build process [18]. It was also observed that for lower values of laser power the hardness value decreases [100]. The increase in hardness also occurs due to an increase in the density

and refinement of the microstructure. The high laser power acts as aging heat treatment to the previously deposited powder layers and thus precipitates the γ' phase which reduces the dislocation and thus increasing the hardness values [120]. Various methods in addition to Vickers hardness like Rockwell, Brinell hardness have been use for mechanical characterization in SLM processes [101]. The average value of hardness of SLM manufactured IN 718 was found to be around 450 ± 30 HV [98, 121].

2.3.3. Geometry Deviation in Selective Laser Melted IN718

IN718 finds its applications widely in the aerospace and bio engineering industries. This demands for high accuracy parts with an improved dimensional accuracy and material characteristics [122]. The process parameters like scanning speed and the laser power affect the geometrical accuracy of the build part [123]. The magnitude of the energy density is multiple of the laser scan speed (v) and laser power (P). Therefore, a change in either of the two above-stated process parameters, a geometric deviation is evident. It was also noted that the increase in laser power (P) causes a decrease in the dimensional accuracy [124]. Over exposure of the metal powder by the laser can lead to defects like balling [125]. Under exposure shall also lead to remnant un-melted powder, which detrimentally effects the mechanical properties of the part by inducing unwarranted porosity [124]. The geometrical deviation can also be attributed to the preheating of the build plate. Preheating of the build plate shall reduce the thermal gradient in the lower layers of the part thereby reducing the possibility of warping of the part [122]. The penetration of capability of the beam and beam diameter, as the total available energy intensity varies with a change in the diameter of the beam [126]. This shall greatly influence the dimensional accuracy of the part.

2.3.4. Residual Stress in Selective Laser Melted IN718

Residual stresses are a major concern in implementing SLM processes for end-use part production. The generation of residual stress can be segregated into two structural models: temperature gradient mechanism (TGM) and cool down phase model [127]. In the TGM model, the residual stress is said to be generated by the restriction offered by the previously solidified layers to the new molten layer. The cool down phase model theorizes that the residual stresses are generated when the already solidified metal layers

restricts the contraction of the recently melted layer [128]. The fundamental reason for the generation of the residual stress is the thermal gradient during fabrication and rapid solidification. The residual stresses generated in the parts by conventional methods can only be controlled up to an extent. The control of the development of stresses is particularly tedious in IN718 as the possible fabrication methods are casting or powder metallurgy. These fabrication techniques are process based and isolated techniques [129]. Therefore, SLM is a viable operation mechanism to fabricate IN718 simultaneously controlling the stresses developed internally. The residual stresses generated shall cause the part to fail by inducing porosity during the fabrication process. Delamination occurs in SLM fabricated parts, which indicates the presence of residual stress. Inter-layer delamination also occurs if the thermal gradients are too high.

It has been found that part distortions increase with an increase in scanning speed (v) and with an increase in laser power (P). An increase in layer thickness (t) resulted in increased porosity. It has been observed that cantilever geometry parts with maximum density exhibit more part distortions and the lower density parts. This is because the pores tend to relax residual stresses [130]. The energy density constant is obtained by a combination of laser power (P) and scanning speed (v). The effect of varying power and exposure on residual stresses and mechanical properties are studied by [131]. A direct relationship existed between laser power, cooling rates, and temperature gradients and inverse relationship between exposure, cooling rate, and temperature gradients. Lower power (P) and higher exposure combination lead to the lowest stress. Finite Element Analysis (FEA) analysis and experimental values are used to understand the residual stress buildup. Varying the layer thickness leads to an inverse relationship with the cooling rate and residual stress. This is because of the increase in melt pool size with an increase in layer thickness. The change in laser power and scanning speed led to the variation in line energy density which leads to porosity [132]. The deformation of the bars due to residual stress increased from an increase in energy density. It is observed to be more in samples with decreased scanning speed (v) and increased laser power (P). At an energy density of 0.2 J/mm, the specimens are without any pores and the tensile and yield strength are almost comparable to the conventionally produced parts. In the study by [133], fabricated samples with

scan speed (v) varying from 400 mm/s to 1000 mm/s and laser power varying from 100 W to 300 W. The stress values are measured using XRD and hole drilling method. As observed in most of the previous studies increasing laser power and decreasing scan speed leads to an increase in residual stresses. This is consistent on both the top and bottom surface as measured by both the methods. However, the initial stress state of the substrate had a significant impact on the stress state of the part. Parts built on stress-relieving substrates had significantly fewer stress values than parts on the as-built counterparts.

SLM has been developed because of the need to process nearly full dense objects with mechanical properties comparable to those of bulk materials and to avoid lengthy post-processing cycles. Although polymers and metals can be completely molten by a laser beam, the denomination SLM applies specifically for metallic materials. In SLM, nearly full density parts can be produced without the need for post-processing steps, while the same materials can be used as in serial production. Basically, the SLM process is the same as SLS except for the much higher laser energy density required. This is one of the most important aspects of SLM. Very high laser energy serves to completely melt the powder and bond the present layer to the previous one in order to obtain high density parts. However, the heat generated by the laser source should rapidly be transported away from the melt pool in order to limit the mechanism of formation of residual stresses.

2.3.5. Techniques to Measure Residual Stresses

Complex thermal profiles of SLM process make it technically challenging to come up with methods to estimate the value of residual stress in the fabricated parts [134]. Destructive and Nondestructive testing are the two primary classifications of the measurement techniques.

2.3.5.1. Destructive methods:

(i) Contour method:

The contour method is a destructive stress measurement technique that serves as a tool to measure the residual stress profile. In this technique, first, the fabricated parts are scanned using a Co-Ordinate

Measuring Machine (CMM) FaroArm® to obtain scanned data of the coordinate points of the stress-relieving plane. The coordinates are then used to re-model the sample for stress analysis in FEA tools.

(ii) Hole drilling method:

Residual stresses can be measured by means of the hole drilling method. It is suitable to evaluate internal-stress state near the surface. The methods involve introducing a very small hole into a part. Since residual stress relax at the hole location, stresses in the surrounding region change causing strains also to change. A strain gage rosette with three radial grids measures these strains. Residual stresses are given by the theory of Kirsch, adjusted with experimental coefficients for blind hole analysis. Key advantages of the hole drilling method include rapid preparation, versatility of the technique for different materials, and reliability. Conversely, the hole drilling method is limited in depth of analysis and specimen geometry and is at least semi-destructive.

(iii) Vickers Hardness method

The Vickers indentation tests can be performed on each surface of specimens where the force is applied usually measured in gf and all the tests are located near the center of the samples' surface. During the test, the occurrence of non-symmetrical indents is generally easily detected during measurement. If a specimen is simply placed on the stage surface, its back surface must be parallel to its polished surface. Tilting the surface more than 1° from perpendicular results in nonsymmetrical impressions and can produce lateral movement between specimen and indenter. The hardness value obtained from the d1 and d2 values, further discussed in section 3.

2.3.5.2. Non-destructive methods:

(i) X-ray diffraction method

The XRD method of stress measurement involves taking 2θ and $\sin^2\psi$ as ordinate and abscissa axis, the XRD data are plotted for measurements performed on as-built samples. The slope of the 2θ-$\sin^2\psi$ straight line is obtained by linear fitting using an XRD analysis software. The fitted relationship and

corresponding coefficient of determination R^2 are also plotted. Statistics of values obtained from XRD measurements, including the slope and the coefficient of determination (R^2) of the fitted 2θ-$\sin^2\psi$ line as well as the resulting residual stress.

(ii) Neutron diffraction:

The principle used is like that of the well-known X-ray technique [6] in which the internal 'lattice' stress present in a material is obtained from the measured elastic 'lattice' strain it produces in the crystallites of which it is composed. The strain is determined using Bragg's law of diffraction. The principal advantage of using neutrons rather than the more conventional X-rays [6] as a probe of stress lies in the fact that the neutrons can penetrate deeply (-~ 3-4 cm) into metals to determine internal stress within the bulk of the material. In contrast, X-rays can only be used non-destructively to examine stresses in near-surface regions. However, the sample to be examined must be taken to a high-intensity reactor or pulsed neutron source and must be small enough to be accommodated on a diffractometer.

(iii) Digital image correlation

The pixel values and grayscale values of a digital image of an object that is captured by a charge-coupled device (CCD) can be used to calculate the object's displacement. An object is deformed when subjected to a load or displacement, and a digital image can be captured before and after the deformation using CCDs. Subsequently, subsets of images in which the pixels have the same width (w) and height (h) as in the original image can be selected. Each image subset has an area of w × h pixels and a distinct grayscale value. The displacement field (du and dv) can be obtained by comparing the object before and after deformation in the image subset. The stresses in a thin film can be calculated using Stoney's equation.

2.3.6. Techniques to Control Residual Stresses

Various Residual stress mitigation methods have been used to reduce the impact of residual stress. About the SLM process, regulation of process parameters shall impact the magnitude of residual stress greatly [135]. The scan speed (v), laser power (P), layer thickness (t), and hatch spacing (h) shall affect the energy density of the laser. It has been found that part distortions increase with an increase in scanning

speed (v) and with an increase in laser power (P) [136]. An increase in layer thickness (t) resulted in increased porosity. It has been observed that cantilever geometry parts with maximum density exhibit more part distortions and the lower density parts [136-138]. Lower power and higher exposure combination lead to the lowest stress [139]. As mentioned in several in situ and post-processing techniques are used to control the stresses produced, such as laser shock peening, heat treatment, and other machining processes. Preheating the build platform is also a way to control the residual stress buildup, especially in complex geometries [134]. The platform temperature is maintained based on the martensitic temperature range of the alloy, and this eliminates the use of post-process heat treatment to homogenize the microstructure. Laser shock peening can be used as a method to control the tensile stresses on the surface of the component [140]. Although the Surface heat treatment techniques are expensive, they can be used as fatigue improvement technique. Heat treatment procedures like annealing and solution heat treatment can be performed to reduce the residual stress build up in the alloy specimen. The reduction in residual stress thereby promotes the strength of the material leading to an increase in the yield strength values.

Chapter 3. Materials and Methods

This chapter provides the details of material preparation and fabrication procedures carried throughout the current study. These details cover the powder preparation, fabrication of the IN718 alloy parts, and sample preparation for the microstructural characterization, compositional analysis, and mechanical tests performed in this study.

3.1. Part Preparation for AM

The parts with the dimension of 10 x 10 x 15 mm were modeled in a computer-aided design (CAD) software. The CAD models were then converted to triangulated stereolithography (STL) files. It was made sure that during the conversion of the CAD model to STL, no design data was lost, and the original design intent was withheld. Next, the STL files were imported into Materialise Magics (Materialise HQ, Belgium) for support generation. After the generation of customized supports for the parts, the process parameters were assigned to the parts using EOS Print 2 (EOS, Krailling, Germany). Finally, the developed models were fed into the printer for printing.

3.2. Powder Preparation and Fabrication

As-received gas atomized IN718 powder with the composition of Ni (50-55 %), Cr (17 - 21%), Nb (4.75-5.5%) was used for the fabrication of the IN718 parts [141]. The average particle size was around 40 μm. The powder was manually sieved to remove particles larger than 75 μm. The powder was initially stored in the powder dispenser bin, after the sieving procedure. It is made sure the powder was closely packed without any air gaps, to avoid the imperfections during the build process[7].

Figure 4: Sieve Machine by Retsch.

Then, an EOS M290 metal 3d printer equipped with a 400 Watt Ytterbium fiber laser and a building volume of 250 mm x 250 mm x 325 mm were used for the fabrication of IN718 samples. The gap between the re-coater and the build plate was adjusted depending upon the layer thickness. After the alignment, the first layer of powder was spread across the build plate. Then, the high power laser melted the powder in the path preloaded in the original uploaded file. Once the powder was melted, a new layer of powder was spread above the previously solidified layer. The layer path is specific to the scan strategy involved, which in turn defines the raster pattern of the laser. The re-coater returns to the home position for the next layer to be deployed. The re-coater blade not only spreads the powder uniformly but also carries away the excess powder to the collector. Initially, the supports are fabricated, which usually have different process parameters than the actual part. This process continues until all the designated layers are layered and fused, thereby manufacturing the target part.

Figure 5: EOS M290 machine with a 400 W fiber laser.

The components were finally fabricated with 375 layers of printing using the optimum values of the energy density of 67 J/mm^2. The adopted laser power (p=285W), layer thickness (t=40 μm), hatch spacing (h=110 μm), and scan speed (v=960 mm/sec) was kept constant in the entire fabrication process. However, four different scan strategies were adopted, namely:

(i) Chess: The chess scan strategy wherein the exposure is comprised of squares and gaps. The total number of squares is equally divided, and each group of squares is scanned in two distinct and definitive directions. The intermittent weaknesses are exposed in succeeding steps. The dimensions and gaps can be adjusted separately.

(ii) Stripes: The other scan strategy was the stripes scan strategy, where the areas exposed were in strips, composed of stripes exposure pattern. The angle between each layer was changed for every 67$^{o.}$

(iii) Customized: The customized scan strategy adopted was a customized scan strategy, where the angle between the consecutive layers was changed consistently at an angle of 90^o.

(iv) F01: The scan vectors in FO1 scan strategy were divided into shorter scan vectors, thereby dividing the laser pass into multiple phases. The alternating angle used here was 67^o

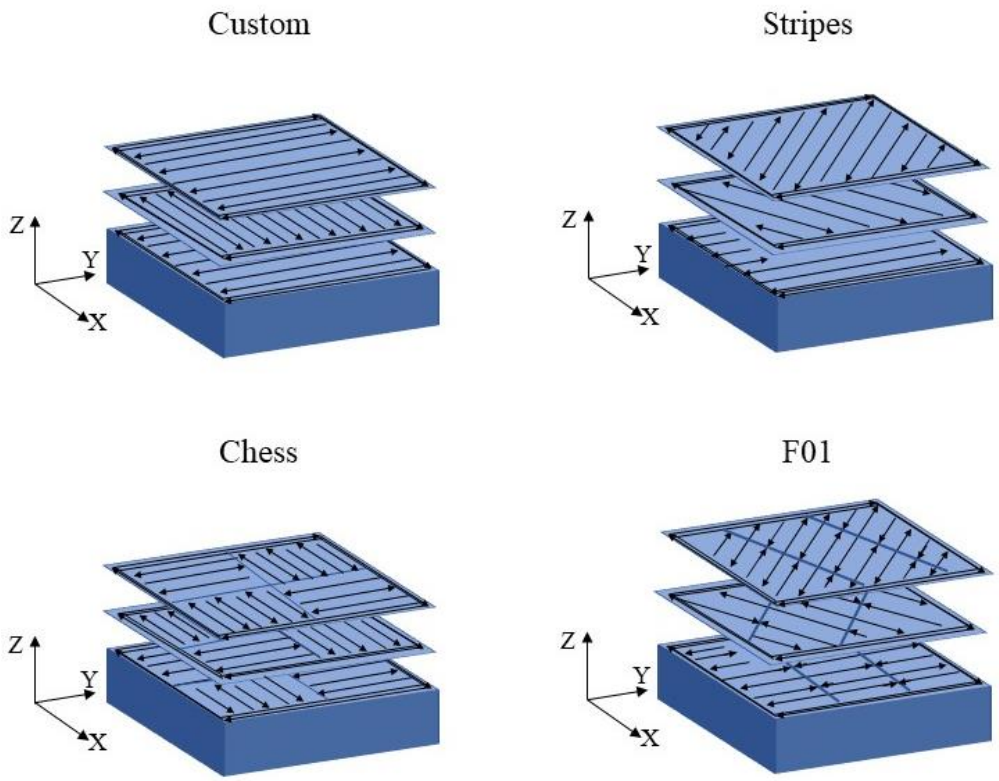

Figure 6: Schematics of scanning strategies (a) Chess (b) Stripes (c) Customized (d) F01.

3.3.Experimental Procedures

In this study, several experiments were performed to reveal the microstructure, mechanical, and metallurgical properties of the fabricated SLM IN718 specimens. These experiments included SEM analysis, hardness measurements, and XRD analysis. The residual stresses were measured using the hardness method.

3.3.1. Sample Preparation

After the fabrication, the samples were separated from the build plate using the band saw. The samples' supports were removed partially during the shearing process, and the remaining supports were removed during the post-processing operations like grinding. The as-built samples were then cut in two different ways: (i) Perpendicular to the build direction with a thickness less than 2 mm for XRD experiments, and (ii) along the build direction through the entire length for 3D scanning using the CMM [142].

Figure 7: Allied Techcut 4 precision cutter.

Furthermore, to achieve an excellent finish on the surface of the fabricated part for SEM analysis, the samples were grinded and polished using the E-prep 4™ (Allied High-Tech Products, Inc., Rancho Dominguez, CA). The samples were first mounted in epoxy resin and then polished using Silicon Carbide (SiC) abrasives, with a varying grit size ranging from 320 to 800. Water was used to convey out the abrasion debris from the spin platen. An XJP- H100 (Amscope, Irvine, CA) metallurgical microscope was used to inspect the samples' surface to check for the uniformity in the abrasive patterns.

Figure 8: E-prep 4™ polisher.

For further polishing, 1 µm diamond suspension on Dia Mat polishing cloth with Green Lube lubricant was used. The final step was performed using 0.04 µm colloidal silica suspension on a Chem-pol polishing cloth. The parts were then removed from the build plate using a band saw. Subsequently, the samples were cleaned using an ultrasonic bath. Compressed air was later used to blow away the debris which was created during handling. The samples were etched with Kroll's Reagent (1-3 mL HF, 2-6 mL HNO3, 100 mL water), before the microstructural analysis.

3.3.2. Scanning Electron Microscope

Hitachi S-3000N Variable Pressure SEM microscopy (Hitachi, Canada) was used for the SEM analysis (Figure 3). The specimens were first mounted on the specimen holder using double-sided carbon tape. The specimen holder's position was fixed using the lock nut and the fastening screw. The samples were placed inside the vacuum chamber, which was later fed into the machine. Finally, the profile and dimensions of the melt pools and grains were evaluated and measured, both near the substrate and away from the substrate, using the SEM. Also, the composition of the formed precipitates was evaluated for the SLM IN718 specimens to reveal the influence of the scanning strategy on the formation of the precipitate. These evaluations were performed for the areas near to the substrates as well as those away from the substrate.

Figure 9: Hitachi S-3000N scanning electron microscope [143].

3.3.3. Coordinate Measuring Machine

Faro arm Quantum^{E} V2 (FARO, Florida, USA) was used to scan the previously sectioned samples. The specific configuration of the Faro Arm was chosen based on the specimen size, weight, and shape of the samples. CMMs measure workpiece dimensions by moving a sensing device, called a probe, in the machine's 3-D measuring envelope, i.e., the X, Y, and Z axes. Noncontact probes were used where a beam of light operating as an optical switch contacted the workpiece. Laser probes projected a laser beam onto the surface of the part, the position of which was then read by triangulation through a lens in the probe receptor. It had a high degree of precision and accuracy.

Figure 10: FARO® QUANTUM FAROARM®.

Once the parts were scanned using the CMM, the scanned point cloud data was imported to Poly Works Inspector (Innvometric, Novi, MI, USA). The additional point cloud information was deleted using the software tool. The scanned part data was then divided into two halves using the reference coordinate systems. Lines were drawn further to separate the part. Then, a total of 10 points were picked on the scanned surface at equally spaced intervals. A matrix of points in a 4x10 distribution was selected. The deflections at each such point were obtained using Poly Works Inspector. The length, width, and height of the part have also been measured for later interpretations for CAD deviation. It is worth noting that the optical noise

generated while scanning the components using the CMM was reduced by coating the sample with a 3D scan spray.

Once the dimensional interpretation of the part was completed, the part model was then replicated in the analysis software. The displacements values that were then obtained from the above-depicted graphs were then set as the load characteristics on the part for the determination of the stresses generated in part.

3.3.4. Hardness Measurements

The Vickers's hardness of SLM IN718 samples was measured by Metal-tester model 900-391D (LECO, St. Joseph's, MI, USA). The sectioned sample was divided into a grid structure of 4x4 on the as-built surface. The hardness indenter was used to measure the hardness at each of the 16 test points on the sample surface. A load of 100 g was selected, and the indenter was moved such that it was on top of the sample, and then the load was applied for a period of 10 seconds. Once the indentation was complete, the indenter was moved again, and the microscopic lens was used to move the crosshairs from one end of the indentation to the other to obtain the values all over the surface. The same procedure was maintained consistently for all the other sample parts. The hardness was further visualized as 3D graphs, with build direction and width of the sample as the axes along with the hardness values. The obtained surface hardness values were also used to calculate the values of residual stresses in part.

Figure 11: LECO LM 300 AT Micro Hardness Tester.

3.3.5. X-ray diffractometer XRD

Crystal and compositional structures of the SLM IN718 samples were determined using a D-500 X-ray diffractometer (Siemens, CA, USA). X-ray source was Cu k-alpha and measurements were made at room temperature (RT) with a wavelength of 1.5418 Å, step intervals of 0.2° in 2Θ between 35° and 110° and speed of 2°/min.

Figure 12: Siemens D500 Powder Diffractometer.

To perform the experiment, the part of the fabricated was sectioned into a sample specimen with a thickness of less than 2mm for it to be accommodated in the sample holder of the XRD machine. The part was then used to perform the compositional analysis. The diffraction angle and the peak intensities were obtained from the XRD data. The sample was swiveled such that the 'Ψ' angle varies at fixed intervals. The intensities at various angles were recorded as a graph of intensity plotted against the diffraction angle. The diffraction angle, intensity, and d-spacing for the highest peak were recorded for calculating the residual stress values in part. Furthermore, the above-stated data was later translated to residual stress. The various' spacing obtained from the graphs discussed earlier was plotted against the $\sin^2\Psi$ value. Finally, the residual

stress was calculated with the slope of the graph being substituted in a mathematical residual stress formulation.

3.3.6. Residual Stress Measurements

Each sample was cut in two, and the contour, or profile, of the resulting new surfaces, were measured to determine the displacements caused by the release of the residual stresses [144].Each sample was cut in two, and the contour, or profile, of the resulting new surfaces, were measured to determine the displacements caused by the release of the residual stresses [144]. For the contour method, the ideal machining process for separating the part would make a precisely straight cut, and the cut plane was assumed to be straight. The ideal machining process for this method is wire EDM, a wire is electrically charged with respect to the workpiece, and spark erosion causes material removal. A finite element model of the beam is created, and the opposite of the measured contour is applied to the surface as a displacement boundary condition.

$$HV \approx 0.1891 \frac{F}{d^2}$$

Where F is the load applied in newtons, and d is the average diagonal distance. The hardness values were calculated from the D1 and D2 values obtained from the test equipment. The residual stress can be calculated using the equation,

$$Rs = K * |s|^{a} * e^{\frac{c^2-1}{0.32}} - 1$$

Where,

$$s = \left(\frac{H}{3.4*K}\right)^{\frac{1}{a}} - 0.08$$

S: Strain due to recovery

K: constant of mechanical testing

C2: ratio of areas

H: Hardness of the material

Chapter 4. Results and Discussion

4.1. Microstructure Analysis

The melt pools of the fabricated parts were observed under a scanning electron microscope and represented in Figure 13. The melt pools were examined along the build direction of the part as the laser scanning path creates visible melt pool regions in each deposited layer continuously melting and fusing the alloy feed powder. Before delving into the analysis of melt pool characteristics, it is necessary to understand the underlying metallurgical implications in SLM. The dimensions of the melt pools are affected by the laser power and velocity of the scan vector. If the laser power is increased, the penetration depth of the laser shall increase, thereby resulting in deeper melt pools. This high energy density results in deep melt pools, which in turn give out tightly packed structures with increased density. Deeper melt pools imply that the previously solidified layer is re-melted to a certain extent based on the laser intensity. This promotes the epitaxial bonding between two consecutive layers, thereby impacting the mechanical properties like hardness and tensile strength. Prolonged exposure (low scan speed), which results in deeper melt pools, also affects the phase composition of the part. This can be attributed to the protracted thermal cycles, which originate due to deeper melt pools. High temperature shall result in the conversion of the strength hardening phases to develop and further transform into the metastable δ phase. The composition of SLM IN718 is further analyzed about scanning strategies as the discussion progresses further. Now, without the loss of generality, it is safe to assert that lower laser power or high scan speed shall result in shallower melt pools and, therefore, less intense thermal gradients.

The melt pool depths of the various fabricated samples were measured and reported in Table 2. The samples fabricated using a chess scan strategy had the deepest melt pools. The samples of stripes and custom strategy exhibited similar melt pool depths. The FO1 scan strategy had the shallowest melt pools when compared to the samples fabricated using other fabrication techniques. The melt pool depth of the sample built using a chess scan strategy was observed to be 89 μm. The depths of melt pools of the Stripes and

Custom scan strategies were 49 μm and 46 μm, respectively. As mentioned above, the average depth of the melt pool of the FO1 sample was measured to be 45 μm.

Although both the chess and custom scan strategy is fundamentally alternated at 90° for each layer, a considerable variation in the melt pool depths is evident. This can be associated with the fact that the custom strategy has a longer scan vector path; therefore, leading to a higher cooling rate. As the far end of the scan, the vector is cooled quickly as the laser traverses along the predefined path, the melt pool begins to solidify. On the other hand, the chess scan strategy is comprised of numerous individual islands, which create localized heat zones. The heat zones shall aid in sustaining the thermal fields generated in the heat-affected zone for more extended periods. This relatively high-temperature layer is recoated with another layer of powder. Now, as the newer layer is being scanned, the previous layer is re-melted as residual heat from the last vector scan adds to the current laser power, thereby increasing the size of the melt pool significantly.

In the striped and FO1 scan strategies, the alternating angle for each layer is 67°. The melt pool depths of both the strategies above are comparable. It was found that the FO1 scan strategy depicted a uniformity in the melt pool depth. This is due to the periodical segmentation of the scan vector in the FO1 scan strategy, which reduced the travel distance of the laser beam, creating shorter scan vectors with smaller thermal gradients in the layer. This led to the uniformity in the melt pool created. Unlike the FO1 scan strategy, the laser traverses the designated path without any discontinuities. This is similar to that of the custom scan strategy, where the thermal gradients are high, and deformations are excessive. The uniformity in the melt pool distribution led to the geometrical stability of the part in the FO1 sample, which exhibited the least amount of geometrical deviation from the designed CAD model.

Considering the custom and stripes strategy, stripes sample had slightly deeper melt pools when compared to the custom strategy. This can be due to the variation in the rastering angle for each layer. The impact of the temperature gradients on the melt pool shall become more comprehensible if the effect of Argon gas flow and sputtering phenomenon are also considered.

Custom
Alternating 90°

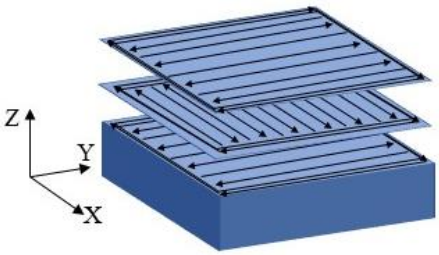

Chess
Alternating 90°

Stripe
Alternating 67°

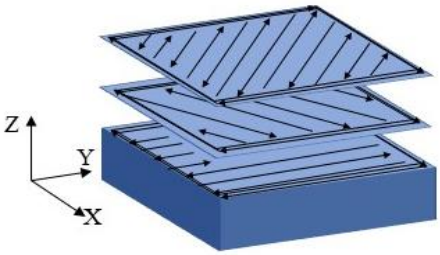

F01
Alternating 67°

Figure 13. Melt pools for the four samples fabricated by different scan strategies: (a) Custom, (b) Chess, (c) Striped, (d) F01. Maximum melt pool depth was found for Chess strategy, and FO1 had the least melt pool depth.

Table 2. Melt pool depth and width for the four samples fabricated by different scan strategies: (a) Custom, (b) Chess, (c) Striped, (d) F01.

Rastering Angle	Scan Strategy	Melt Pool Depth (µm)	Melt Pool Width (µm)
Alternating 90°	Custom	46	132
	Chess	79	140
Alternating 67°	Stripe	49	135
	F01	45	120

Figure 14 represents the grain structures of the specimens fabricated with different scan strategies. The sample fabricated using FO1 strategy, had cellular, non-dendritic grains at the melt pool boundaries. The higher thermal gradient in the layer, led to rapid solidification of the melt pool. Therefore, the rapid solidification aids in the formation of cellular grain structures. On the other hand, the chess scan strategy exhibited the presence of elongated grains when compared to FO1 scan strategy. The prolonged thermal cycles in the chess strategy, reduce the thermal gradient. The decelerated heat loss gives rise to elongated grains. The deeper melt pools foster the grain growth in the build direction thereby leading to striated grain structures. Parts with smaller grains have improved strength as the surface area of the grains is low, thereby reducing the possibility of dislocations in the grain structure. This is true as the dislocations in the grain are contained within the edges of grain boundaries. This renders strength to the specimen with smaller grains [145]. Therefore, the FO1 sample specimen, shall analytically exhibit improved strength when compared to that of Chess strategy.

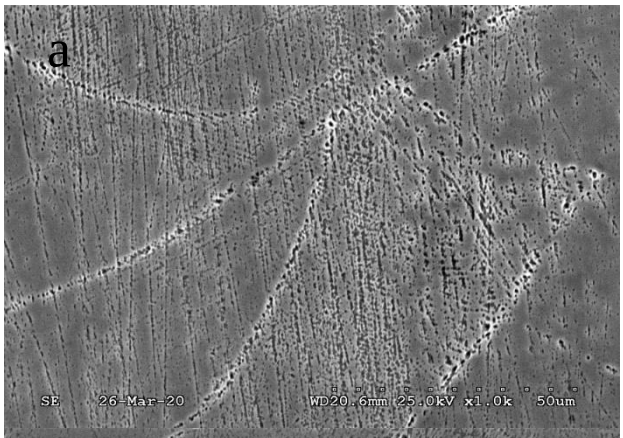

Custom
Alternating 90°

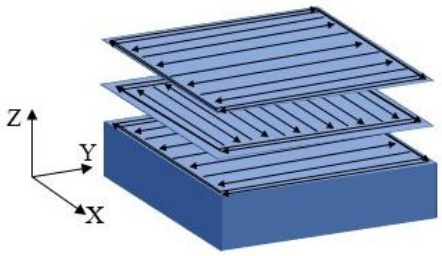

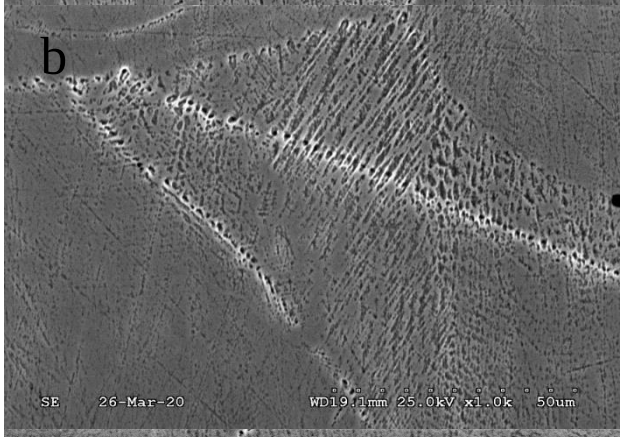

Chess
Alternating 90°

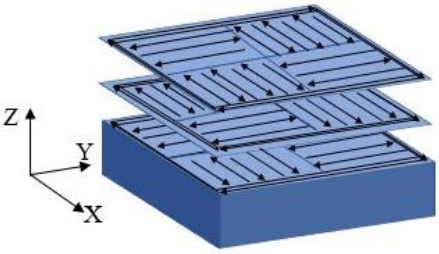

Stripe
Alternating 67°

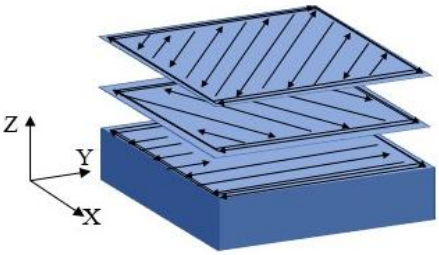

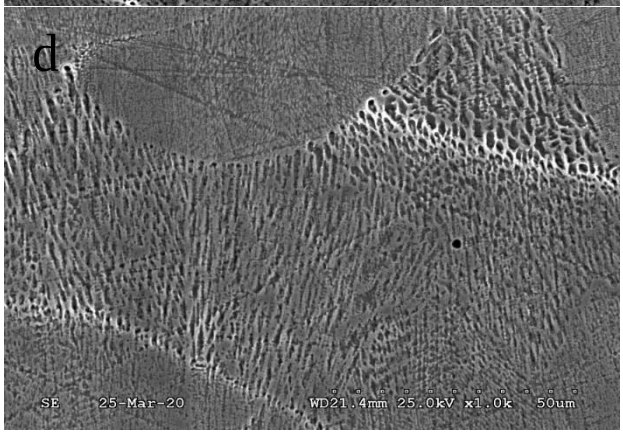

F01
Alternating 67°

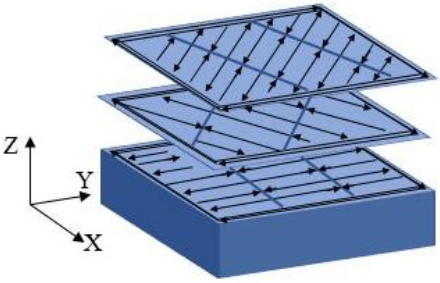

Figure 14. Grain structure for the four samples fabricated by different scan strategies: (a) Custom, (b) Chess, (c) Striped, (d) F01. The F01 showed the formation of cellular grain structures while the chess scan strategy exhibited the presence of elongated grains.

4.2. Geometrical Deviation

The geometrical deviation of the four used scan strategies in three co-ordinate directions was measured, and the percentage deviation between the built dimension and the actual part dimension was recorded. Firstly, in terms of length, the Flow Optimization (FO1) scan strategy has the least geometric deviation. However, a significantly higher variation can be seen in the chess scan strategy employed sample. The average deviation of the chess strategy is also considerably higher when compared to that of the FO1 scan strategy. This can be attributed to the increase in the number of localized heat zones in the Chess strategy. As the laser requires time to attain the pre-defined laser speed, the energy delivered to each scan island is higher in Chess strategy. This leads to the presence of a higher number of heating zones. As the number of heating zones is increased, then there is an increase in the geometrical deviations. The deeper melt pools observed in the sample of chess scan strategy, augment the higher geometrical deviation observed in part.

The FO1 scan strategy shows lesser geometrical deviations due to the presence of shallower melt pools. FO1 scan strategy has shown the least dimensional deviation among striped, custom, and chess scan strategies. The average deviation in FO1 is 0.73%, which is lower than that of 1.11% of stripes strategy. The longer scan vectors in striped scan strategy, have a higher thermal gradient when compared to that of the shorter scan vectors of the FO1 scan strategy.

The other scan strategies like stripe, custom, and FO1 have a relatively low difference in percentage deviation when compared to the chess scan strategy. The longer scan vectors have a smaller number of localized heat zones, thereby reducing the overall thermal gradient. The laser requires additional time during travel before reaching the defined parameters like scan speed. Therefore, the properties of such regions in the layer shall have different metallurgical properties. During the time expended for the laser to traverse the distance below the preassigned velocity, the energy input, or the thermal energy given to the

part is higher [146]. This leads to the formation of deeper melt pools, which in return, impact the dimensions of the as-built part. This shall also lead to a higher temperature gradient, thereby increasing the stresses generated during the cooling phase of the melting process. The higher energy input leads to increased epitaxial bonding in part. From the obtained dimensional analysis, the highest deviation is in terms of height; this is due to the aforementioned epitaxial bonding between layers. Although some research suggests that the chess scan strategy shall have less geometric distortion as the specific energy density increases, employing this scanning strategy leads to micro porosity and cracks, which shall directly impact the build of the part [146, 147].

The deviation values in both Custom and Striped strategies are similar as the scan vectors are longer in both the scan strategies. In the case of stripes strategy, the length of the scan vector varies throughout the hatch pattern. In a custom scan pattern, the hatching is consistently rotated by an angle of 90°, thereby maintaining uniformity in the scan vector length. This minor variation in lengths of the scan vector can be considered as the reason for the higher deviation in dimensions in stripes strategy when compared to custom scan strategy.

Table 3: The CAD deviation of the four samples along x, y, z.

Dimension	***% Deviation***			
	Custom	**Chess**	**Stripes**	**F01**
Length	0.8	0.8	0.7	0.2
Width	0.8	1.2	0.5	0.2
Height	1.6	2.4	2.1	1.8
Average % deviation	1.1	1.5	1.1	0.7

4.3. XRD Analysis

The XRD results of the IN718 specimens fabricated with different scanning strategies are demonstrated in Figure 15. The compositional analysis of the samples showed the presence of γ phase, γ′ phase, γ’’ phase, δ phase, and Laves. In all specimens, it was found that the composition of IN718 constituted mainly of Ni, Cr, Fe, Nb, Ti, Al, and Mo. The Ni (Cr, Fe) γ phase primarily have Ni and Cr

elements. The γ′ phase, comprised of Ni_3 (Al, Ti), is one of the primary strengthening phases which are coherent with the γ base phase and has a Face Centered Cubic (FCC) crystal structure. The presence of Nb is conducive to the formation of the γ″ (Ni_3Nb), another strengthening phase, which has a body centered tetragonal BCT crystal structure. The XRD analysis of the IN718 alloy also shows the presence of another subsidiary phase 'δ' which is formed due to rapid cooling. The δ phase is a precipitate phase which arises due to the thermal morphology of γ″. The γ″ is the primary strengthening phase in the alloy, but the transformation of γ″ into the δ phase is not always beneficial. One of the fundamental limitations of IN718 is the reduction in strengthening properties under high temperatures due to δ precipitation as the Nb is separated at the grain boundaries. As the composition of the δ and γ″ phase are the same, the fabrication temperatures are of primal importance to control the strength of the part and its other physical properties. Principally, the primary alloying elements like Mo, Ta, W, and Reconstitute the Laves phase. Although the Laves are formed in the specimens, it can be conveniently transformed into the γ″ phase to alleviate the brittle nature of the sample by using post-process heat treatment at elevated temperatures. The laves phase results in the segregation of alloying elements like Nb, hence rendering it as an extra element rather than using it as a strength-building component. It is noteworthy that the elevated temperatures pose a risk of further transforming into another precipitate δ upon prolonged exposure.

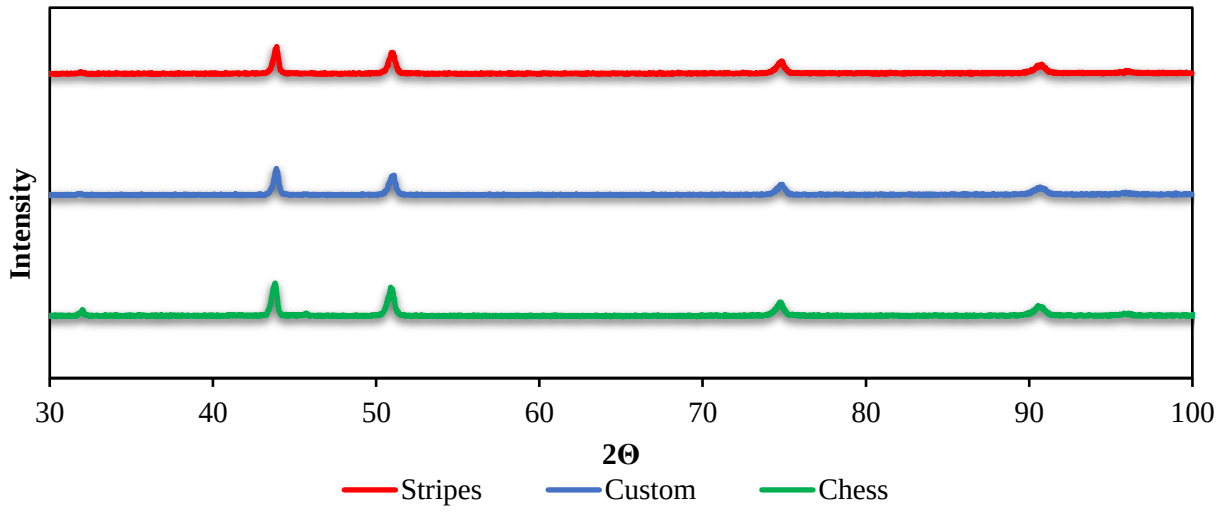

Figure 15. XRD graph of phases of the four samples fabricated by different scan strategies: (a) Custom, (b) Chess, and (c) Striped.

Details about the phases detected by XRD measurements are reported in Table 3. The chess scan strategy exhibited a significantly high proportion of γ′ and γ″, therefore hold a high value of hardness. On the other hand, the stripes, custom, and FO1 scan strategies have a relatively lower hardness value as the percentage of the strengthening phases is significantly lower. As chess scan strategy had the highest exposure time in terms of laser passes, the γ′ and γ″ phases are predominant. However, higher the presence of γ″ means that the parts have lower applicability at elevated temperatures. The compositional analysis shows that the strengthening phases can be directly correlated to the hardness of the specimen. Therefore, the application of the parts or sample is the predominant driving factor to tailor the internal metallurgical configuration, as the physical conditions shall influence the overall performance of the specimen.

Table 4. XRD compositional analysis of the four samples fabricated by different scan strategies: (a) Custom, (b) Chess, and (c) Striped.

Scan Strategy	Peak	γ Area	γ Area (%)	γ' Area	γ' Area (%)	γ'' Area	γ'' Area (%)
Custom	1	86.6	79.9	11.1	10.3	10.6	9.8
	2	75.0	66.6	32.4	28.8	5.2	4.6
	3	31.8	74.1	6.3	14.7	4.8	11.2
	4	52.7	63.5	17.1	20.6	13.1	15.8
	5	8.1	62.1	2.6	19.7	2.4	18.2
Total		254.2	***70.6***	69.6	***19.3***	36.2	***10.0***
Chess	1	0.0	0.0	134.7	80.1	33.5	19.9
	2	0.0	0.0	0.0	0.0	5.5	100.0
	3	77.0	61.7	39.9	32.0	7.9	6.4
	4	68.7	77.1	20.4	22.9	0.0	0.0
	5	49.3	73.4	0.0	0.0	17.8	26.6
	6	0.0	0.0	0.0	0.0	3.9	100.0
	7	8.7	55.1	5.1	32.0	2.0	12.9
Total		203.7	***42.9***	200.0	***42.2***	70.7	***14.9***
Stripes	1	72.4	75.4	20.9	21.7	2.8	2.9
	2	109.4	73.1	21.1	14.1	19.2	12.8
	3	33.2	72.7	7.4	16.2	5.1	11.1
	4	43.9	62.1	13.5	19.1	13.3	18.8
	5	5.4	61.2	1.5	17.7	1.9	21.2
Total		264.2	***71.2***	64.4	***17.4***	42.2	***11.4***

4.4. Hardness Analysis

Pertaining to this analysis, four scan strategies have been employed while printing the IN718 parts. The overall hardness values of the parts exhibit a valid trend. As seen in Figure 12, the parts fabricated using the chess scan strategy have the highest total average hardness value of 421.4 HV. Basically, in the SLM process, the top portion of each solidified layer would be re-melted in combination with the newly deposited powder layer, which aids in the epitaxial bonding between two layers. The degree of re-melting, however, highly depends on the scan strategy employed during the fabrication. Deeper melt pools correspond to a higher degree of re-melting. As previously discussed, the magnitude of the depth of the melt pools in the chess scan strategy is high, which leads to epitaxial bonding between various layers; this, in turn, increases the hardness of the part. In SLM specimens where the melt pools are deeper, thermal cycles would be maintained for long, and hence the secondary phases would be more predominantly existent. Thus, the higher value of hardness observed in the Chess scan strategy can be attributed to the higher amounts of the strengthening phases such as γ' and γ'' in the as-built IN718 part. On the other hand, as seen in Figure 12, the Vickers' hardness of the specimens other than the chess scan strategy has lower hardness values, with FO1 being the least at 374.1 HV. In these three scan strategies, the inter and intralayer thermal transactions do not sustain heat for a prolonged time, thus resulting in lower amounts of the strengthening phases in the as-built part. A correlation between the hardness and the chemical composition is discussed in further sections with insights into the XRD analysis.

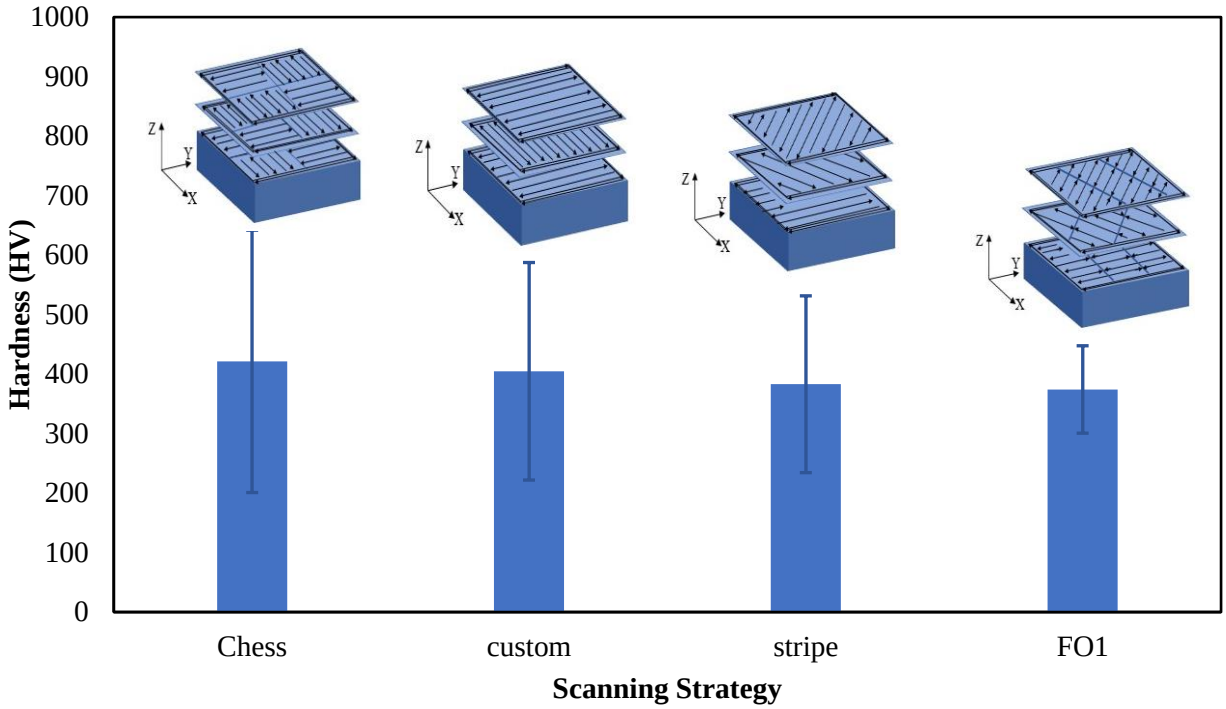

Figure 16. Hardness plot for (a) Custom, (b) Chess, (c) Striped, (d) F01.

4.5. Residual Stress- Hardness Method

The primary reason for residual stress during SLM fabrication can be attributed to temperature gradient developed in and around the close vicinity of the heat-affected zone (HAZ). This thermal gradient then causes the inter-layer deformation as a rapid cooling ensues as the laser beam traverses further away. This deformation not only effects the inter-layer bonding but also influences the geometric conformation of the as-built part. The delamination shall lead to crack formation. These cracks are detrimental during the build, as they cause the part to detach from the build platform during the fabrication process, thereby rendering the fabrication effort to be a failure.

The samples which were fabricated using the chess and FO1 scan strategies exhibited high residual stress values of 594 MPa and 586 MPa. Coincidentally, both these scan strategies were unconventional scan strategies, where the laser scan vectors were split into shorter scan paths. As discussed earlier, the inter layer heat accumulation in these strategies is higher. This shall lead to numerous internal distortions in the layers of the part. The stripes and custom scan strategies, have longer scan vectors and lower heat

encapsulation, thereby reducing the residual stress accumulation in the parts. The stress generated in the stripes and custom strategies is 504 MPa and 520 MPa. Although the heat accumulation is favorable to mitigate stress in SLM parts, the stress value shall increase in case of increase energy encapsulation, which leads to delamination and instill a variation into microstructure and mechanical properties. Studies conducted on re-melting of the previously deposited layer like [148] have found supportive results which show an increase in thermal intensities in beneficial for an extent. However, exploitation of the above stated fact shall result in an increase in the residual stress build up in the part. The increase in the residual stress value can be explained by considering the laser absorptivity of the powder and the solidified part. The powder particles more readily absorb the laser energy as the surface area is higher when compared to the solidified layer. Therefore, the energy imparted in a single square might not be sufficient to completely re-melt the previous layer. Usually, the as seen from the micro graphs the energy is high enough to obtain deeper melt pools. This additional entrapped heat in the part, contributes to an increase in residual stress values in chess and FO1 scan strategies. Various techniques like build plate reheating, re-melting of the layers to a certain extent, further optimization of process parameters, and altering the scan strategies can be adopted.

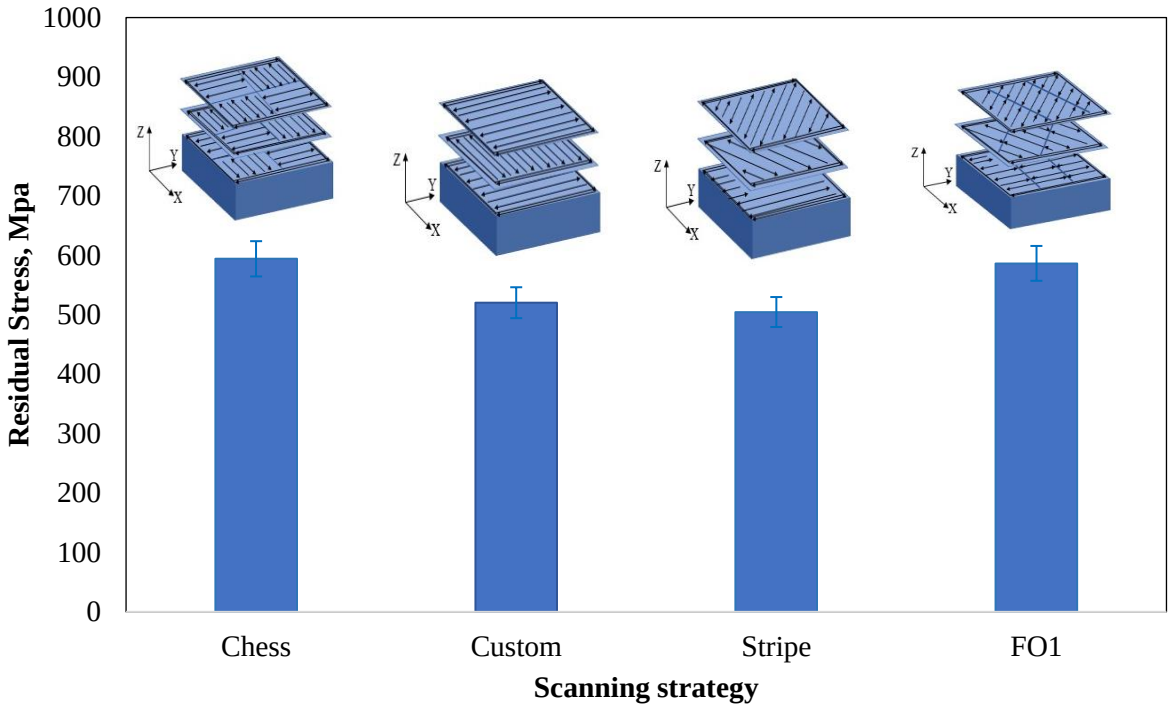

Figure 17. Residual Stress plot for (a) striped scan strategy, (b) custom scan strategy, (c) chess, and (d) F01.

Chapter 5. Conclusions and Future Works

5.1. Conclusions

After conducting the experimental and microstructural analysis,

(i) Higher geometrical deviations were observed for parts built with chess scan strategy and parts fabricated using FO1 strategy showed the least deformations in part dimensions. This can be attributed to the presence of deeper melt pools in chess strategy samples which facilitate epitaxial grain growth in the part. The stripes and custom scan strategies exhibited lower dimensional deviations as the time expended during the laser attains the pre-defined velocity also impacts the final shape of the part.

(ii) The deeper melt pools in the samples fabricated using Chess scan strategy imparted high hardness to the part by increasing in the proportion of the strength hardening phases in the part. The highest percentage of γ' and γ'' values were found in the chess scan strategy sample which had the highest hardness value.

(iii) The highest values of residual stress were observed in the sample built using the chess scan strategy. The residual stress of FO1 scan strategy was also close to that of chess strategy. This can be associated to the phenomenon of laser re-melting and laser absorptivity. The stripes and custom scan strategies had relatively low stress values as the localized heat zones are less prominent.

5.2. Future Work

This study has investigated the effect of laser scan strategy on the microstructure, mechanical properties and residual stress of Inconel 718 parts fabricated by selective laser melting. Some of the potential avenues of research that can be considered are:

- The residual stress reduction methods like re-melting, build plate heating and in-situ monitoring of the heat zones in the part shall aid in better comprehending the effects of the thermal interactions and their effect on residual stress generated in the part.

- Modelling novel scanning strategies to reduce the defects in the parts, namely porosity, cracks and residual stresses.
- The microstructural analysis for the porosity and the density measurement can provide better insights into the effect of scanning strategies on the part properties.

References

[1] L. Zheng, G. Schmitz, Y. Meng, R. Chellali, R. Schlesiger, Mechanism of Intermediate Temperature Embrittlement of Ni and Ni-based Superalloys, Critical Reviews in Solid State and Materials Sciences (2012).

[2] D.F. Paulonis, J.J. Schirra, Alloy 718 at Pratt & Whitney–Historical perspective and future challenges, Superalloys (2001).

[3] H. Dabbaghi, M. Nematollahi, K.S. Baghbaderani, P. Bayatimalayeri, M. Elahinia, High-Temperature Oxidation Kinetics of Additively Manufactured NiTiHf, arXiv preprint arXiv:2006.11114 (2020).

[4] S. Metals, Inconel alloy 718, Special Metals, 2007.

[5] L.C. Ardila, F. Garciandia, J.B. Gonzalez-Diaz, P. Alvarez, A. Echeverria, M. Petite, R. Deffley, J. Ochoa, Effect of IN718 Recycled Powder Reuse on Properties of Parts Manufactured by Means of Selective Laser Melting, Physics Procedia 56 (2014) 9.

[6] E.A. Loria, The Status and Prospects of Alloy 718, The Journal of The Minerals, Metals & Materials Society (1988) 6.

[7] D. Deng, Additively Manufactured Inconel 718 : Microstructures and Mechanical Properties, Departement of Management and Engineering, Linköping University, 2018.

[8] V.R. Rajendran, K. Mamidi, B. Ravichander, B. Farhang, A. Amerinatanzi, N.S. Moghaddam, Determination of residual stress for Inconel 718 samples fabricated through different scanning strategies in selective laser melting, Behavior and Mechanics of Multifunctional Materials IX, International Society for Optics and Photonics, 2020, p. 1137719.

[9] S. Srivathsan, B.B. Ravichander, N.S. Moghaddam, N. Swails, A. Amerinatanzi, Investigation of the strength of different porous lattice structures manufactured using selective laser melting, Behavior and Mechanics of Multifunctional Materials IX, International Society for Optics and Photonics, 2020, p. 113771B.

[10] M.J. Donachie, S.J. Donachie, Superalloys: a technical guide, ASM international (2002).

[11] R. Bowman, Superalloys: A Primer and History, 9th International Symposium on Superalloys, Champion, Pennsylvania, 2000.

[12] B. Seitz, METHODOLOGY FOR EFFICIENTLY ESTABLISHING PROCESSING-STRUCTURE-PROPERTY RELATIONSHIPS FOR ADDITIVE-MANUFACTURED AGE-HARDENED ALLOYS, George W. Woodruff School of Mechanical Engineering, Georgia Institute of Technology, 2016.

[13] H.K.D.H. Bhadeshia, Nickel Based Superalloys, (2016).

[14] J.M. Oblak, D.F. Paulonis, D.S. Duvall, Coherency strengthening in Ni base alloys hardened by DO_{22} γ' precipitates, Metallurgical Transactions (1974).

[15] S. Azadian, L.-Y. Wei, R. Warren, Delta phase precipitation in Inconel 718, Materials Characterization 53(1) (2004).

[16] J.K.Hong, J.H.Park, N.K.Park, I.S.Eom, M.B.Kim, C.Y.Kang, Microstructures and mechanical properties of Inconel 718 welds by CO_2 laser welding, Journal of Materials Processing Technology 201(1-3) (2008).

[17] J. Strößner, M. Terock, U. Glatzel, Mechanical and Microstructural Investigation of Nickel-Based Superalloy IN718 Manufactured by Selective Laser Melting (SLM), Advanced Engineering Materials (2015).

[18] Q. Jia, D. Gu, Selective laser melting additive manufacturing of Inconel 718 superalloy parts: Densification, microstructure and properties, Journal of Alloys and Compunds 585 (2014).

[19] A.A. Popovich, V.S. Sufiiarov, I.A. Polozov, E.V. Borisov, Microstructure and mechanical properties of Inconel 718 produced by SLM and subsequent heat treatment, Key Engineering Materials (2015).

[20] D. Zhang, W. Niu, X. Cao, Z. Liu, Effect of standard heat treatment on the microstructure and mechanical properties of selective laser melting manufactured Inconel 718 superalloy, Materials Science and Engineering: A 644 (2015).

[21] P. Scallan, Material evaluation and process selection, Process Planning (2003).

[22] J. Li, Z. Zhao, P. Bai, H. Qu, B. Liu, L. Li, L. Li, L. Wu, R. Guan, H. Liu, Z. Guo, Microstructural evolution and mechanical properties of IN718 alloy fabricated by selective laser melting following different heat treatments, Journal of Alloys and Compunds 772 (2019) 10.

[23] R.G. Carlson, J.F. Radavich, MICROSTRUCTURAL CHARACTERIZATION OF CAST 718 International Symposium on Superalloys, 1989.

[24] G.A. Rao, M. Kumar, M. Srinivas, D.S. Sarma, Effect of standard heat treatment on the microstructure and mechanical properties of hot isostatically pressed superalloy Inconel 718, Materials Science and Engineering: A (2003).

[25] H. Dabbaghi, K. Safaei, M. Nematollahi, P. Bayati, M. Elahinia, Additively Manufactured NiTi and NiTiHf Alloys: Estimating Service Life in High-Temperature Oxidation, Materials 13(9) (2020) 2104.

[26] G.A. Rao, M. Srinivas, D.S. Sarma, Influence of modified processing on structure and properties of hot isostatically pressed superalloy Inconel 718, Materials Science and Engineering: A (2006).

[27] G.A. Rao, M. Srinivas, D.S. Sarma, Effect of oxygen content of powder on microstructure and mechanical properties of hot isostatically pressed superalloy Inconel 718, Materials Science and Engineering: A (2006).

[28] M. Elahinia, N.S. Moghaddam, M.T. Andani, A. Amerinatanzi, B.A. Bimber, R.F. Hamilton, Fabrication of NiTi through additive manufacturing: A review, Progress in Materials Science 83 (2016) 630-663.

[29] A. Jahadakbar, M. Nematollahi, K. Safaei, P. Bayati, G. Giri, H. Dabbaghi, D. Dean, M. Elahinia, Design, Modeling, Additive Manufacturing, and Polishing of Stiffness-Modulated Porous Nitinol Bone Fixation Plates Followed by Thermomechanical and Composition Analysis, Metals 10(1) (2020) 151.

[30] N.S. Moghaddam, S.E. Saghaian, A. Amerinatanzi, H. Ibrahim, P. Li, G.P. Toker, H.E. Karaca, M. Elahinia, Anisotropic tensile and actuation properties of NiTi fabricated with selective laser melting, Materials Science and Engineering: A 724 (2018) 220-230.

[31] N.S. Moghaddam, A. Jahadakbar, A. Amerinatanzi, M. Elahinia, Recent advances in laser-based additive manufacturing, Laser-Based Additive Manufacturing of Metal Parts, CRC Press2017, pp. 1-24.

[32] G.G. Berdine, M. DiPaola, M. Weinberg, Economic and Regulatory Perspectives on Additive Manufacturing, 3D Printing in Orthopaedic Surgery, Elsevier2019, pp. 41-48.

[33] M. Attaran, The rise of 3-D printing: The advantages of additive manufacturing over traditional manufacturing, Business Horizons 60(5) (2017).

[34] I. Gibson, D. Rosen, B. Stucker, Additive Manufacturing Technologies, 2 ed.2015.

[35] M.T. Andani, N.S. Moghaddam, C. Haberland, D. Dean, M.J. Miller, M. Elahinia, Metals for bone implants. Part 1. Powder metallurgy and implant rendering, Acta biomaterialia 10(10) (2014) 4058-4070.

[36] B. Baufeld, E. Brandl, O. Van der Biest, Wire based additive layer manufacturing: Comparison of microstructure and mechanical properties of Ti–6Al–4V components fabricated by laser-beam deposition and shaped metal deposition, Journal of Materials Processing Technology 211(6) (2011) 1146-1158.

[37] C. Deckard, J. Beaman, Selective Laser Sintering, Birth of an Industry, 2012.

[38] C.R. Deckard, Method and apparatus for producing parts by selective sintering, USA, 1986.

[39] J.M. Pearce, C.M. Blair, K.J. Laciak, R. Andrews, A. Nosrat, I. Zelenika-Zovko, 3-D Printing of Open Source Appropriate Technologies for Self-Directed Sustainable Development Journal of Sustainable Development 3 (2010).

[40] EOS-GmbH, History, 2014. http://www.eos.info/about_eos/history.

[41] L.-E. Andersson, M. Larsson, DEVICE AND ARRANGEMENT FOR PRODUCING A THREE-DIMENSIONAL OBJECT Arcam AB, USA, 2001.

[42] B. Berman, 3-D printing: The new industrial revolution, Business Horizons 55 (2012).

[43] B. Xiao, Y. Zhang, Laser sintering of metal powders on top of sintered layers under multiple-line laser scanning, Journal of Physics D: Applied Physics 40 (2007).

[44] B. Baufeld, E. Brandl, O.V.d. Biest, Wire based additive layer manufacturing: Comparison of microstructure and mechanical properties of Ti–6Al–4V components fabricated by laser-beam deposition and shaped metal deposition, Journal of Materials Processing Technology (2011).

[45] P.J. Andersen, S.K. Hodson, Articles of manufacture and methods for manufacturing laminate structures including inorganically filled sheets, USA, 1998.

[46] D. Ding, Z. Pan, D. Cuiuri, H. Li, A multi-bead overlapping model for robotic wire and arc additive manufacturing (WAAM), Robotics and Computer-Integrated Manufacturing 31 (2015).

[47] I. Gibson, David Rosen, and Brent Stucker, "Directed energy deposition processes." Additive Manufacturing Technologies, (2015).

[48] R.a.S.Z. Goodridge, "Powder bed fusion of polymers." Laser Additive Manufacturing, (2017) 181-204.

[49] A. MT, S.M. N, H. C, D. D, M. MJ, E. M, Metals for bone implants. Part 1. Powder metallurgy and implant rendering, Acta Biomater (2014).

[50] M.H. Elahinia, Shape Memory Alloy Actuators: Design, Fabrication and Experimental Evaluation, John Wiley & Sons2015.

[51] I.V. Shishkovsky, L.T. Volova, M.V. Kuznetsov, Y.G. Morozov, I.P. Parkin, Porous biocompatible implants and tissue scaffolds synthesized by selective laser sintering from Ti and NiTi. Journal of Materials Chemistry, Journal of Materials Chemistry (12) (2008).

[52] M.H. Elahinia, M. Hashemi, M. Tabesh, S.B. Bhaduri, Manufacturing and processing of NiTi implants: A review, Progress in Materials Science 57(5) (2012).

[53] S.C. Danforth, M. Agarwala, A. Bandyopadghyay, N. Langrana, V.R. Jamalabad, A. Safari, R.V. Weeren, Solid freeform fabrication methods, USA, 1998.

[54] A. Bandyopadhyay, T.P. Gualtieri, S. Bose, Global Engineering and Additive Manufacturing, Additive Manufacturing (2015) 1.

[55] M. Khaing, J. Fuh, L. Lu, Direct metal laser sintering for rapid tooling: processing and characterisation of EOS parts, Journal of Materials Processing Technology 113(1) (2001) 269-272.

[56] S. Kolossov, E. Boillat, R. Glardon, P. Fischer, M. Locher, 3D FE simulation for temperature evolution in the selective laser sintering process, International Journal of Machine Tools and Manufacture 44(2) (2004) 117-123.

[57] M. Agarwala, D. Bourell, J. Beaman, H. Marcus, J. Barlow, Direct selective laser sintering of metals, Rapid Prototyping Journal 1(1) (1995) 26-36.

[58] J.-P. Kruth, X. Wang, T. Laoui, L. Froyen, Lasers and materials in selective laser sintering, Assembly Automation 23(4) (2003) 357-371.

[59] J. Goban, M. Semancík, T. Lazoríková, Manufacturing of forms for injection moulding technology by rapid prototyping method, Annals of the Faculty of Engineering Hunedoara 11(1) (2013) 195.

[60] Iamchaitanya, SLM, [https://iamchaitanya.wordpress.com/2015/07/22/powder-metallurgy/]done

. Iamchaitanya, Website, 2020.

[61] M. Shellabear, O. Nyrhilä, DMLS-Development history and state of the art, Laser Assisted Netshape Engineering 4, Proceedings of the 4th LANE (2004) 21-24.

[62] I. Gibson, D.W. Rosen, B. Stucker, Additive manufacturing technologies, Springer2010.

[63] D. Gu, Y.-C. Hagedorn, W. Meiners, G. Meng, R.J.S. Batista, K. Wissenbach, R. Poprawe, Densification behavior, microstructure evolution, and wear performance of selective laser melting processed commercially pure titanium, Acta Materialia 60(9) (2012) 3849-3860.

[64] I. Yadroitsev, I. Smurov, Selective laser melting technology: from the single laser melted track stability to 3D parts of complex shape, Physics Procedia 5 (2010) 551-560.

[65] S. Huang, F. You, H. Peng, W. Luo, Y. Feng, S. Lv, L. Sun, C. Yan, Influence of surface on spectroscopic properties of rare earth ions in nanocrystals, Journal of Rare Earth 25(4) (2007) 396-401.

[66] M. Elahinia, N.S. Moghaddam, M.T. Andani, R. Rahmanian, J. Walker, M. Miller, D. Dean, Site-specific material properties and the additive manufacturing of nitinol musculoskeletal implants, Tissue Engineering Part A, MARY ANN LIEBERT, INC 140 HUGUENOT STREET, 3RD FL, NEW ROCHELLE, NY 10801 USA, 2014, pp. S120-S121.

[67] A. Amerinatanzi, H. Zamanian, N. Shayesteh Moghaddam, A. Jahadakbar, M. Elahinia, Application of the superelastic NiTi spring in ankle foot orthosis (AFO) to create normal ankle joint behavior, Bioengineering 4(4) (2017) 95.

[68] N. Moghaddam, A. Amerinatanzi, S. Saedi, A. Turabi, H. Karaca, M. Elahinia, Stiffness Tuning of Niti Implants Through Aging, V001T02A014-V001T02A014 (2016).

[69] N.S. Moghaddam, A. Jahadakbar, A. Amerinatanzi, M. Elahinia, Recent Advances in Laser Based Additive Manufacturing Laser-Based Additive Manufacturing of Metal Parts, Taylor & Francis Group2017.

[70] M. Aliakbari, Additive manufacturing: State-of-the-art, capabilities, and sample applications with cost analysis, (2012).

[71] R. Udroiu, POWDER BED ADDITIVE MANUFACTURING SYSTEMS AND ITS APPLICATIONS, Academic journal of manufacturing engineering 10(4) (2012).

[72] V. Petrovic, J. Vicente Haro Gonzalez, O. Jordá Ferrando, J. Delgado Gordillo, J. Ramón Blasco Puchades, L. Portolés Griñan, Additive layered manufacturing: sectors of industrial application shown through case studies, International Journal of Production Research 49(4) (2011) 1061-1079.

[73] S. Saedi, A.S. Turabi, M.T. Andani, N.S. Moghaddam, M. Elahinia, H.E. Karaca, Texture, aging, and superelasticity of selective laser melting fabricated Ni-rich NiTi alloys, Materials Science and Engineering: A 686 (2017) 1-10.

[74] R. Rahmanian, N.S. Moghaddam, C. Haberland, D. Dean, M. Miller, M. Elahinia, Load bearing and stiffness tailored niti implants produced by additive manufacturing: a simulation study, Behavior and Mechanics of Multifunctional Materials and Composites 2014, International Society for Optics and Photonics, 2014, p. 905814.

[75] A. Jahadakbar, N. Shayesteh Moghaddam, A. Amerinatanzi, D. Dean, H.E. Karaca, M. Elahinia, Finite element simulation and additive manufacturing of stiffness-matched niti fixation hardware for mandibular reconstruction surgery, Bioengineering 3(4) (2016) 36.

[76] A. Dehghanghadikolaei, H. Ibrahim, A. Amerinatanzi, M. Hashemi, N.S. Moghaddam, M. Elahinia, Improving corrosion resistance of additively manufactured nickel–titanium biomedical devices by micro-arc oxidation process, Journal of materials science 54(9) (2019) 7333-7355.

[77] N.S. Moghaddam, M. Elahinia, M. Miller, D. Dean, Enhancement of bone implants by substituting nitinol for titanium (Ti-6Al-4V): A modeling comparison, Smart Materials, Adaptive Structures and Intelligent Systems, American Society of Mechanical Engineers, 2014, p. V001T03A031.

[78] H.D. Dean, M.H. Elahinia, C. Haberland, M.J. Miller, A. Sutradhar, N.S. Moghaddam, J.M. Walker, R. Skoracki, Methods, devices, and manufacture of the devices for musculoskeletal reconstructive surgery, Google Patents, 2017.

[79] A. Hadi, M. Qasemi, M. Elahinia, N. Moghaddam, Modeling and experiment of a flexible module actuated by shape memory alloy wire, Smart Materials, Adaptive Structures and Intelligent Systems, American Society of Mechanical Engineers, 2014, p. V001T03A035.

[80] B. Raad, N.S. Moghaddam, M. Elahinia, A numerical simulation of the effect of using porous superelastic Nitinol and stiff Titanium fixation hardware on the bone remodeling, Nanosensors, Biosensors, and Info-Tech Sensors and Systems 2016, International Society for Optics and Photonics, 2016, p. 98021T.

[81] K.A. Mumtaz, P. Erasenthiran, N. Hopkinson, High density selective laser melting of Waspaloy®, Journal of materials processing technology 195(1) (2008) 77-87.

[82] B. Zhang, H. Liao, C. Coddet, Microstructure evolution and density behavior of CP Ti parts elaborated by self-developed vacuum selective laser melting system, Applied surface science 279 (2013) 310-316.

[83] L. Dong, H. Wang, Microstructure and corrosion properties of laser-melted deposited Ti2Ni3Si/NiTi intermetallic alloy, Journal of Alloys and Compounds 465(1-2) (2008) 83-89.

[84] B. Zhang, H. Liao, C. Coddet, Selective laser melting commercially pure Ti under vacuum, Vacuum 95 (2013) 25-29.

[85] S. Saedi, S.E. Saghaian, A. Jahadakbar, N.S. Moghaddam, M.T. Andani, S.M. Saghaian, Y.C. Lu, M. Elahinia, H.E. Karaca, Shape memory response of porous NiTi shape memory alloys fabricated by selective laser melting, Journal of Materials Science: Materials in Medicine 29(4) (2018) 40.

[86] A. Ahmadi, N. Shayesteh Moghaddam, M. Elahinia, H.E. Karaca, R. Mirzaeifar, Finite element modeling of selective laser melting 316l stainless steel parts for evaluating the mechanical properties, International Manufacturing Science and Engineering Conference, American Society of Mechanical Engineers, 2016, p. V002T01A003.

[87] N.S. Moghaddam, A. Jahadakbar, M. Elahinia, D. Dean, M. Miller, The effect of adding dental implants to the reconstructed mandible comparing the effect of using Ti-6Al-4V and NiTi hardware, Tissue

Engineering Part A, MARY ANN LIEBERT, INC 140 HUGUENOT STREET, 3RD FL, NEW ROCHELLE, NY 10801 USA, 2015, pp. S398-S398.

[88] S. Thakare, B.B. Ravichander, N. Swails, N.S. Moghaddam, A. Amerinatanzi, The effect of support structure geometry on surface topography of selectively laser melted parts, Behavior and Mechanics of Multifunctional Materials IX, International Society for Optics and Photonics, 2020, p. 113771D.

[89] A. Jahadakbar, N.S. Moghaddam, A. Amerinatanzi, D. Dean, M. Elahinia, Mechanical evaluation of the SLM fabricated, stiffness-matched, mandibular bone fixation plates, Behavior and Mechanics of Multifunctional Materials and Composites XII, International Society for Optics and Photonics, 2018, p. 1059610.

[90] N.S. Moghaddam, S. Saedi, A. Amerinatanzi, E. Saghaian, A. Jahadakbar, H. Karaca, M. Elahinia, Selective laser melting of Ni-rich NiTi: selection of process parameters and the superelastic response, Behavior and Mechanics of Multifunctional Materials and Composites XII, International Society for Optics and Photonics, 2018, p. 105960W.

[91] M.J. Ashrafi, A. Amerinatanzi, Z. Saebi, N.S. Moghaddam, R. Mehrabi, H. Karaca, M. Elahinia, Shape memory response of cellular lattice structures: Unit cell finite element prediction, Mechanics of Materials 125 (2018) 26-34.

[92] K.S. Baghbaderani, M. Nematollahi, P. Bayatimalayeri, H. Dabbaghi, A. Jahadakbar, M. Elahinia, Mechanical Evaluation Of Selective Laser Melted Ni-Rich Niti: Compression, Tension, And Torsion, arXiv preprint arXiv:2006.15659 (2020).

[93] P. Mercelis, J.-P. Kruth, Residual stresses in selective laser sintering and selective laser melting, Rapid Prototyping Journal 12(5) (2006) 254-265.

[94] H. Exner, M. Horn, A. Streek, F. Ullmann, L. Hartwig, P. Regenfuß, R. Ebert, Laser micro sintering: A new method to generate metal and ceramic parts of high resolution with sub-micrometer powder, Virtual and Physical Prototyping 3(1) (2008) 3-11.

[95] P. Regenfuss, L. Hartwig, S. Klotzer, R. Ebert, H. Exner, Microparts by a novel modification of selective laser sintering, TECHNICAL PAPERS-SOCIETY OF MANUFACTURING ENGINEERS-ALL SERIES- (2004).

[96] P. Regenfuss, L. Hartwig, S. Klötzer, R. Ebert, T. Brabant, T. Petsch, H. Exner, Industrial freeform generation of microtools by laser micro sintering, Rapid Prototyping Journal 11(1) (2005) 18-25.

[97] N.S. Moghaddam, S. Saedi, A. Amerinatanzi, A. Hinojos, A. Ramazani, J. Kundin, M.J. Mills, H. Karaca, M. Elahinia, Achieving superelasticity in additively manufactured NiTi in compression without post-process heat treatment, (2019).

[98] Z. Wang, K. Guan, M. Gao, X. Li, X. Chen, X. Zeng, The microstructure and mechanical properties of deposited-IN718 by selective laser melting, Journal of Alloys and Compunds 513 (2012) 6.

[99] B. Farhang, B.B. Ravichander, F. Venturi, A. Amerinatanzi, N.S. Moghaddam, Study on variations of microstructure and metallurgical properties in various heat-affected zones of SLM fabricated Nickel-Titanium alloy, Materials Science and Engineering: A 774 (2020).

[100] K.N. Amato, S.M. Gaytan, L.E. Murr, E. Martinez, P.W. Shindo, J. Hernandez, S. Collins, F. Medina, Microstructures and mechanical behavior of Inconel 718 fabricated by selective laser melting, Acta Materialia 60(5) (2012).

[101] E. Chlebus, K. Gruber, B. Kuźnicka, J.Kurzac, T.Kurzynowski, Effect of heat treatment on the microstructure and mechanical properties of Inconel 718 processed by selective laser melting, Materials Science and Engineering: A 639 (2015).

[102] F. Brenne, A. Taube, M. Pröbstle, S. Neumeier, D. Schwarze, M. Schaper, T. Niendorf, Microstructural design of Ni-base alloys for high-temperature applications: impact of heat treatment on microstructure and mechanical properties after selective laser melting, Progress in Additive Manufacturing (2016).

[103] M. Pröbstle, S. Neumeier, J. Hopfenmüller, L. Freund, T. Niendorf, D. Schwarze, M. Göken, Superior creep strength of a nickel-based superalloy produced by selective laser melting, Materials Science and Engineering: A (2016).

[104] O. Es-Said, J. Foyos, R. Noorani, M. Mendelson, R. Marloth, B. Pregger, Effect of layer orientation on mechanical properties of rapid prototyped samples, Materials and Manufacturing Processes 15(1) (2000) 107-122.

[105] M. Elahinia, N.S. Moghaddam, A. Amerinatanzi, S. Saedi, G.P. Toker, H. Karaca, G.S. Bigelow, O. Benafan, Additive manufacturing of NiTiHf high temperature shape memory alloy, Scripta Materialia 145 (2018) 90-94.

[106] A. Ahmadi, R. Mirzaeifar, N.S. Moghaddam, A.S. Turabi, H.E. Karaca, M. Elahinia, Effect of manufacturing parameters on mechanical properties of 316L stainless steel parts fabricated by selective laser melting: A computational framework, Materials & Design 112 (2016) 328-338.

[107] C. Ma, M.T. Andani, H. Qin, N.S. Moghaddam, H. Ibrahim, A. Jahadakbar, A. Amerinatanzi, Z. Ren, H. Zhang, G.L. Doll, Improving surface finish and wear resistance of additive manufactured nickel-titanium by ultrasonic nano-crystal surface modification, Journal of Materials Processing Technology 249 (2017) 433-440.

[108] H. Ibrahim, A. Jahadakbar, A. Dehghan, N.S. Moghaddam, A. Amerinatanzi, M. Elahinia, In vitro corrosion assessment of additively manufactured porous NiTi structures for bone fixation applications, Metals 8(3) (2018) 164.

[109] S.N. Esfahani, M.T. Andani, N.S. Moghaddam, R. Mirzaeifar, M. Elahinia, Independent tuning of stiffness and toughness of additively manufactured titanium-polymer composites: Simulation, fabrication, and experimental studies, Journal of Materials Processing Technology 238 (2016) 22-29.

[110] N.S. Moghaddam, A. Jahadakbar, A. Amerinatanzi, M. Elahinia, M. Miller, D. Dean, Metallic fixation of mandibular segmental defects: Graft immobilization and orofacial functional maintenance, Plastic and Reconstructive Surgery Global Open 4(9) (2016).

[111] N.S. Moghaddam, M.T. Andani, A. Amerinatanzi, C. Haberland, S. Huff, M. Miller, M. Elahinia, D. Dean, Metals for bone implants: Safety, design, and efficacy, Biomanufacturing Reviews 1(1) (2016) 1.

[112] S. Saedi, N.S. Moghaddam, A. Amerinatanzi, M. Elahinia, H.E. Karaca, On the effects of selective laser melting process parameters on microstructure and thermomechanical response of Ni-rich NiTi, Acta Materialia 144 (2018) 552-560.

[113] N.S. Moghaddam, R. Skoracki, M. Miller, M. Elahinia, D. Dean, Three dimensional printing of stiffness-tuned, nitinol skeletal fixation hardware with an example of mandibular segmental defect repair, Procedia CIRP 49 (2016) 45-50.

[114] N. Shayesteh Moghaddam, Toward patient specific long lasting metallic implants for mandibular segmental defects, University of Toledo, 2015.

[115] S.S.N.E. Munaganuru, Muthu Ram Prabhu & Vadlamudi, Vamsee & Shaik, Rauhon Ahmed & Adluru, Hari Kishore & Raihan, Md Rassel & Reifsnider, Kenneth. , Effects of Build Parameters on the Mechanical and Di-Electrical Properties of AM parts., ((2018)).

[116] K. Mamidi, H.K. Talla, B.B. Ravichander, B. Farhang, N.S. Moghaddam, A. Amerinatanzi, Study on the influence of post-processing parameters over microstructure and metallurgical properties of NiTi alloy, Behavior and Mechanics of Multifunctional Materials IX, International Society for Optics and Photonics, 2020, p. 113770V.

[117] A. Loghman, H. Shayestemoghadam, Magneto-thermo-mechanical creep behavior of nano-composite rotating cylinder made of polypropylene reinforced by MWCNTs, Journal of Theoretical and Applied Mechanics 54(1) (2016) 239-249.

[118] A. Loghman, H. Shayestemoghadam, E. Loghman, Creep evolution analysis of composite cylinder made of polypropylene reinforced by functionally graded MWCNTs, (2016).

[119] M.E. Aydinöz, F. Brenne, M. Schaper, C. Schaak, W. Tillmann, J. Nellesen, T. Niendorf, On the microstructural and mechanical properties of post-treated additively manufactured Inconel 718 superalloy under quasistatic and cyclic loading, Materials Science and Engineering: A (2016).

[120] X. Gong, X. Wang, Z. Jones, K. Cooper, J.V. Cole, K. Chou, Characterization of Microstructure and Mechanical Property of Inconel 718 from Selective Laser Melting, ASME 2015 International Manufacturing Science and Engineering Conference, Charlotte, North Carolina, 2015.

[121] B.B. Ravichander, B. Farhang, N. Swails, A. Amerinatanzi, N.S. Moghaddam, Analysis of the deviation in properties of selective laser melted samples fabricated by varying process parameters, Behavior and Mechanics of Multifunctional Materials IX, International Society for Optics and Photonics, 2020, p. 113771A.

[122] D. Buchbinder, W. Meiners, N. Pirch, K. Wissenbach, J. Schrage, Investigation on reducing distortion by preheating during manufacture of aluminum components using selective laser melting, Journal of Laser Applications (2014).

[123] M. Sadowski, L. Ladani, W. Brindley, J. Romano, Optimizing quality of additively manufactured Inconel 718 using powder bed laser melting process, Additive Manufacturing 11 (2016).

[124] Q. Shi, D. Gu, M. Xia, S. Cao, T. Rong, Effects of laser processing parameters on thermal behavior and melting/solidification mechanism during selective laser melting of TiC/Inconel 718 composites, Optics and Lasers Technology 84 (2016).

[125] X. Han, H. Zhu, X. Nie, G. Wang, X. Zeng, Investigation on Selective Laser Melting AlSi10Mg Cellular Lattice Strut: Molten Pool Morphology, Surface Roughness and Dimensional Accuracy, Materials (2018).

[126] D. Wang, S. Wu, Y. Bai, H. Lin, Y. Yang, C. Song, Characteristics of typical geometrical features shaped by selective laser melting, Journal of Laser Applications (2017).

[127] Z.Y.L. C. Li , X.Y.Fang , Y.B.Guo Residual stress in metal additive manufacturing Elsevier (2018) 348-353.

[128] Y.Z. Wei Gao, Devarajan Ramanujan, Karthik Ramania, Yong Chen,, C.C.L.W. Christopher B. Williams, Yung C. Shin, Song Zhan,, P.D. Zavattieri, The status, challenges, and future of additive manufacturing in

engineering, (2015) 65-89.

[129] Y.Z. Wei Gao, Devarajan Ramanujan, Karthik Ramani, Yong Chen,, C.C.L.W. Christopher B. Williams, Yung C. Shin, Song Zhang,, P.D. Zavattieri, The status, challenges, and future of additive manufacturing in

engineering, Elsevier (2015

) 65-89.

[130] D.D. L. Mugwagwa, S.Matope, I. Yadroitsev, Influence of process parameters on residual stress related distortions in Selective Laser melting Elsevier (2018) 92-99.

[131] H.G. Haider Ali, Kamran Mumtaz, Processing Parameter Effects on Residual Stress and mechanical properties of selective laser melted Ti6Al4V, CrossMark 27(8) (2018).

[132] Effect of laser energy density on the microstructure, mechanical properties and deformation of Inconel 718 samples fabricated by Selective Laser melting, Elsevier (2019) 481-488.

[133] I.A. J. Robinson, P. Fox, E. Jones, C. Sutcliffe, Determination of the effect of scan strategy on residual stress in laser, Elsevier (2018) 13-24.

[134] S.S. Bo Cheng, Kevin Chou, Stress and deformation evaluations of scanning strategy effect in

selective laser melting, Elsevier (2016) 240-251.

[135] H.G. Haider Ali, Kamran Mumtaz, Processing Parameter Effects on Residual Stress

and Mechanical Properties of Selective Laser Melted

Ti6Al4V, cross mark (2017) 4059-4068.

[136] D.D. L. Mugwagwa, S. Matope, I. Yadroitsev, Influence of process parameters on residual stress related distortions in selective laser melting, (2018) 92-99.

[137] Z.J.Z. H.Y. Wan, C.P. Li,G.F. Chen,G.P. Zhang, Effect of scanning strategy on mechanical properties of selective laser melted

Inconel 718, Elsevier (2019) 42-48.

[138] H.Y.W.Z.J.Z.C.P.L.G.F.C.G.P. Zhang, Effect of scanning strategy on grain structure and crystallographictexture of Inconel 718 processed by selective laser melting, Elsevier (2018) 1799-1804.

[139] S.C. Naresh Nadammal , Tatiana Mishurova , Tobias Thiede , Arne Kromm,, L.F. Christoph Seyfert , Christoph Haberland , Judith Ann Schneider ,, G.B. Pedro Dolabella Portella Effect of hatch length on the development ofmicrostructure, texture and

residual stresses in selective laser melted superalloy Inconel 718, Elsevier (2017) 139-150.

[140] I.A.A. L.A. Parry, R.D. Wildman, Geometrical effects on residual stress in selective laser melting, Elsevier (2019).

[141] EOS, https://www.eos.info/en/additive-manufacturing/3d-printing-metal/dmls-metal-materials/nickel-alloys.

[142] N.S. Moghaddam, A. Jahadakbar, A. Amerinatanzi, R. Skoracki, M. Miller, D. Dean, M. Elahinia, Fixation Release and the Bone Bandaid: A New Bone Fixation Device Paradigm, Bioengineering (2017).

[143] http://www.phys-astro.sonoma.edu/people/faculty/shi/kecklab/sem.htm.

[144] S.W. Yanjin Lu, Yiliang Gan, Tingting Huang, Chuanguang Yang, Lin Junjie, Jinxin Lin Study on the microstructure, mechanical property and residual stress of SLM Inconel-718 alloy manufactured by differing island scanning strategy.

[145] Materials Principles and Practice Electronic Materials Manufacturing with Materials Structural Materials, 1990.

[146] F.G. A.M. Mancisidor, M. San Sebastian, P. Alvarez, J. Diaz, I. Unanue, Reduction of the residual porosity in parts manufactured by selective laser meltingusing skywriting and high focus offset strategies, (2016).

[147] H.G. Haider Ali, Kamran Mumtaz, Effect of scanning strategies on residual stress and mechanical properties ofSelective Laser Melted Ti6Al4V, (2018).

[148] J.V.R.D.G.R.J.M.H.S.D.R.C.S. Edmondson, The effect of laser remelting on the surface chemistry of Ti6al4V components fabricated by selective laser melting, (2016).